Spring 2010

Experimental and Numerical Investigations on Aerodynamic Characteristics of Savonius Wind Turbine with Various Overlap Ratios

Khandakar Niaz Morshed

EXPERIMENTAL AND NUMERICAL INVESTIGATIONS ON AERODYNAMIC CHARACTERISTICS OF SAVONIUS WIND TURBINE WITH VARIOUS OVERLAP RATIOS

by

KHANDAKAR NIAZ MORSHED

(Under the Direction of Mosfequr Rahman)

ABSTRACT

Savonius wind turbine is the simplest type of vertical axis rotor that has a relatively low efficiency. Operation of the Savonius wind turbine is based on the difference of the drag force on its semi-spherical blades, depending on whether the wind is striking the convex or the concave part of the blades. This turbine is being used in various countries around the world due to the simplistic design, cheap technology for construction, and a good starting torque independent of wind direction at low wind speeds. Due to its simple design and low construction cost, this rotor is mainly used for water pumping as well as wind power on small scale. The main goal of this current research is to investigate the aerodynamic performance of Savonius wind turbine. Wind tunnel investigation was carried out to find the aerodynamic characteristics like, drag coefficient, torque coefficient, and power coefficient of three blade Savonius wind turbine rotor models with and without overlap ratio (ratio of overlap distance between two adjacent blades and rotor diameter ,OR = a/D) at various Reynolds numbers. Numerical investigation was also carried out to find those aerodynamic characteristics. For numerical investigation, commercial computational fluid dynamic (CFD) software GAMBIT and FLUENT were used. Afterwards those two results were compared for verification. Three different models with different overlap ratio were designed and

fabricated for the current study to find the effect of overlap ratios. The results from the experimental part of the research show a significant effect of overlap ratio and Reynolds number on the improvement of aerodynamic performance of the Savonius wind turbine. At higher Reynolds number turbine Model without overlap ratio gives better aerodynamic coefficients and at lower Reynolds number Model with moderate overlap ratio gives better results.

EXPERIMENTAL AND NUMERICAL INVESTIGATIONS ON AERODYNAMIC CHARACTERISTICS OF SAVONIUS WIND TURBINE WITH VARIOUS OVERLAP RATIOS

by

KHANDAKAR NIAZ MORSHED

B.Sc. Bangladesh University of Engineering and Technology, Bangladesh, 2005

A Thesis Submitted to the Graduate Faculty of Georgia Southern University in

Partial Fulfillment of the Requirements for the Degree

MASTERS OF SCIENCE

STATESBORO, GEORGIA

2010

EXPERIMENTAL AND NUMERICAL INVESTIGATIONS ON AERODYNAMIC CHARACTERISTICS OF SAVONIUS WIND TURBINE WITH VARIOUS OVERLAP RATIOS

by

KHANDAKAR NIAZ MORSHED

Major Professor:	Mosfequr Rahman
Committee:	Aniruddha Mitra
	Hung-Ming Cheng
	Scott Kersey

Electronic Version Approved:
May 2010

DEDICATION

This work is dedicated to my parents who gave me the mental support to overcome challenges.

ACKNOWLEDGEMENTS

I would like to express my sincere gratitude to my advisor Dr. Mosfequr Rahman for his valuable guidance, direction and encouragement throughout the progress of this research at Georgia Southern University. I would like to express my gratitude to Dr. Aniruddha Mitra, Dr. Hung-Ming Cheng and Dr. Scott Kersey for their participation as members of my supervisory committee.

Special gratitude goes to Andrew Michaud for helping me fabricating the turbine models and also to Jonathan Turner, Jeff Lewis and Mark Fuller to helping build the wind tunnel.

LIST OF SYMBOLS

Symbol	Explanation
A	Rotor area
D	Overall rotor diameter
d	Blade diameter
H	Rotor height
a	Overlap distance between two adjacent blades
V	Wind velocity, m/s
N	Revolution per minute
ν	Kinematic viscosity, m^2/s
ρ	Air density, kg/m^3
OR	Overlap ratio: ratio of overlap distance between two adjacent blades and rotor diameter (OR = a/D)
AR	Aspect ratio
ω	Angular velocity, rad/sec
Re	Reynolds Number
λ	Tip speed ratio
T	Torque
P	Power

Δp	Pressure difference
F_l	Lift force
F_n	Normal drag force
F_t	Tangential drag force
C_n	Normal drag coefficient
C_t	Tangential drag coefficient
C_q	Torque Coefficient
C_p	Power Coefficient
C_l	Lift Coefficient

TABLE OF CONTENTS

LIST OF TABLES

Table Page

LIST OF FIGURES

CHAPTER 1

INTRODUCTION

General

With the rising demand of energy, conventional energy is becoming more expensive and scarce. The need to generate power from renewable sources to reduce the demand for fossil fuels and the damage of their resulting carbon dioxide emissions is now well understood. So there is an obvious need for alternative sources of energy. Renewable energy sources include wind energy, solar energy, tidal energy, geothermal energy, and biomass energy. Wind is among the most popular sources of alternative energy because it is pollution free and available almost any time of the day, especially in the coastal regions. As a sustainable energy resource, electrical power generation from the wind is increasingly important in national and international energy policy in response to climate change. The main advantages of wind energy include its availability year round, no green house gases, and domestic availability. The disadvantages of wind energy are high installation cost and the necessity of strong winds to produce electricity.

The two primary types of wind turbine are the horizontal axis wind turbine (HAWT) and vertical axis wind turbine (VAWT). HAWTs include both upwind and downwind configurations, with various performance enhancers, such as diffusers and concentrators. HAWTs are the most popular configuration now because they have higher efficiency, but they are only suitable for places with extremely strong, gusty winds and urban areas [29]. In contrast, VAWTs work well in places with relatively low wind strength, and constant winds [29]. HAWTs are highly developed and used in all large-scale wind farms. Most research on VAWT design was carried

out as long ago as the late 1970s and early 1980s. Interest dropped after HAWTs were determined to be more efficient at large scale, and very little research probed VAWT aerodynamics or sought to resolve the problem of the interaction of its blade structure with unsteady aerodynamic loads. Their technical development lags significantly behind that of HAWTs. However, HAWTs have never been proven fundamentally more aerodynamically efficient than VAWTs. Indeed, VAWTs may be more appropriate than HAWTs on a very large scale (10MW+) when the alternating gravitational loading on a HAWT blade becomes excessive. VAWTs have a number of advantages over HAWTs. First, they do not have to constantly yaw into the local wind direction. Second, due to their relatively lower rotational speed, they are typically quieter. Third, the cost of manufacturing very large VAWTs could be lower due to their simple, straight, constant section blades as compared to the HAWTs' complex, three-dimensional blades and, for the same reason, they could be easier to manufacture. Finally, VAWTs are mechanically better able to withstand high winds because their stalling behavior changes, offering a potential safety advantage during gust conditions. VAWTs include both a drag-type configuration, such as the Savonius rotor, and a lift-type configuration, such as the Darrieus rotor.

Savonius Wind Turbines

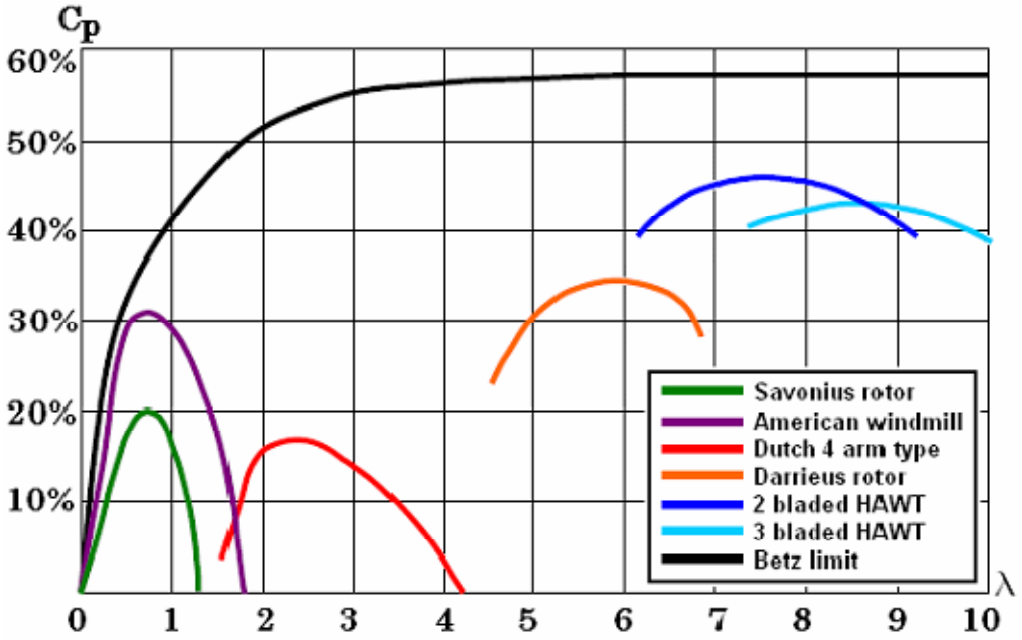

Figure 1.1: Power coefficient (Cp) versus Tip speed ratio (λ) for various Wind Turbines [19].

The Savonius wind turbine is the simplest. Its operation depends on the difference in drag force when the wind strikes either the convex or concave part of its semi-spherical blades. It is good at self-starting and works independently of wind direction. However, its efficiency is relatively lower than that of the lift-type VAWTs. Due to its simple design and low construction cost, Savonius rotors are primarily used for water pumping and to generate wind power on a small scale, and its large starting torque makes it suitable for starting other types of wind turbines that have inferior starting characteristics, such as the Darrieus rotor and Gyro mill [11]. Recently, some generators with high torque at low rotational speed, suitable for small-scale wind turbines, have been developed, suggesting that Savonius rotors may yet be used to generate electric power [11].

Moreover, in low cut in wind speeds Savonius wind turbine gives very high starting torque. For this characteristic Savonius wind turbine is used with another turbine (i.e. Darrieus wind turbine) with poor starting torque. Menet et al. [20] have shown using L-σ criterion that Savonius rotor has more mechanical stress resistance than a horizontal axis wind turbine. Figure 1.1 compares the performance of Savonius wind turbine (power coefficient, C_p) with other conventional types of wind turbine.

Wind Energy Utilization

Energy experts predict that by proper development of wind energy they can meet up to 20% of U.S. energy demand [35]. To make the wind energy viable, some challenges must be overcome. To produce 20% of the nation's energy from wind by 2030, generation capacity must be increased to 305 GW [35]. According to U.S. energy reports, US wind power generation capacity in 2006 was 11.6 GW [35]. By 2008, it had grown to 25 GW, 8 GW more than in 2007 [24]. World wind power generation capacity in 2007 was estimated at 95 GW, which is 40% higher than previous year [36]. Germany is currently leading in wind energy generation capacity, followed by Spain and the United States. China vowed to reach the mark of 30 GW by 2020. India sets a target of 10.5 GW by 2012 [36].

Scope of Research

Researchers from different parts of the world have been investigating the aerodynamic characteristics of Savonius wind turbine and tried to identify the optimum design of it which can give better performance compared to HAWTs. Although much research has been going on experimentally and numerically on Savonius wind turbine performance improvement,

comprehensive study using both experimental and numerical methods for various gap ratios at different Reynolds number has not been extensively studied, if studied at all. In this current research three bladed Savonius wind turbine models with different gap ratios will be investigated experimentally and numerically at various Reynolds number. Both pressure difference method and direct static torque measurement method have been performed for experimental investigation on performance improvement of the three bladed Savonius wind turbine. For numerical investigation commercial available software FLUENT and GAMBIT have been used.

Objectives of the Present Study

The primary goal of the present study is to investigate the aerodynamic characteristics of three bladed Savonius wind turbines in order to contribute in the performance improvement of vertical axis wind turbine (VAWT). To achieve this goal the following objectives were set for the present study:

i. Design and fabricate Savonius wind turbine scale models with no overlap ratio and two different overlap ratios;
ii. Measure pressure distribution around the Savonius turbine rotor models and calculate drag coefficients;
iii. Measure static torque using subsonic wind turbine for all models at varying angles of rotation;
iv. Numerically mesh will be generated around all turbine models using GAMBIT;
v. Fluid flow field around the models will be solved using k-ε turbulence model of FLUENT; pressure contours, velocity contours and torque coefficient will be determined at various Reynolds number; and

vi. Using the numerical torque coefficient power coefficient will be calculated and compared with the experimental results.

Outline of the thesis

Chapter 2 provides a brief description of the findings of several researchers both experimental and numerical investigation for different models of Savonius wind turbine at different Reynolds number for different conditions.

Chapter 3 outlines experimental setup, turbine models design development, governing equations, experimental methodology, numerical code validation and numerical methodology. Chapter 4 presents findings of the present study and discussion. Finally, chapter 5 contains conclusion of the current study and suggestion for future work.

CHAPTER 2

LITERATURE REVIEW

Introduction

Significant numbers of researchers have been working to improve the aerodynamic characteristics of Savonius wind turbine. This research are varies from laboratory measurement, full scale simulation to numerical and theoretical prediction for flow around the Savonius wind turbine. Researchers have contributed a lot to the horizontal axis wind turbine and Darrieus vertical axis wind turbine, because of their high potentiality of wind efficiency. So far an extensive amount of research has been done on Savonius wind turbines in order to make the Savonius wind turbine appropriate for small scale use by several researchers around the world. In this chapter a brief discussion of experimental and numerical work on Savonius wind turbines will be discussed.

History of Vertical Axis Wind Turbine

Wind turbines have been used from ancient time. People used wind energy for various purposes. Historians mentioned that the use of windmills probably started around 2000 B.C. The time period ending at the nineteenth century is termed as the ancient development period and the time period from the nineteenth century to present time is termed as the modern development period. The first wind turbine in history produced electricity in Denmark at the end of the nineteenth century; it was a multi bladed horizontal axis wind turbine.

A detailed report and drawings of a vertical axis windmill were given by a Syrian cosmographer Al-Dimashqi about 1300 A.D [34]. It was a two storied wall structure with milestones at the top and a rotor at the bottom. It had latter with spoked reel with 6 to 12 upright ribs that covered with cloth. Wulff [37] found this type of windmill was still in operation in 1963. Wulff estimated the power output of those windmills was about 75 hp (at wind speed 30 m/s) and efficiency was 50%. Each windmill milled one ton of grain in 24 hours [37].

The Savonius wind turbine was first used by a Finnish Engineer S. J. Savonius in 1931 [32]. The design of his rotor was S-shaped with two semi-circular buckets with small overlap. At that time this rotor was successfully used as an ocean current meter. In 1931 G. J. M. Darrieus in France patented another vertical axis wind turbine named Darrieus vertical axis rotor. This type of rotor was not self starting.

Literature review on Experimental investigation

Wind turbine aerodynamics must be designed for optimal output to exploit the wind energy in a specific location. This problem remains both challenging and crucial. Much research has been conducted on Savonius rotors with two semi-cylindrical blades and S-shaped rotors with various flow parameters. Islam et al. [13] investigated the aerodynamic forces acting on a stationary S-shaped rotor and attempted to predict its dynamic performance. They measured the pressure distribution over the surfaces of the blades and found that flow separates over the front and back surfaces, and the point of separation depends on the rotor angle. They also found that the net torque becomes maximum at a rotor angle of $\alpha = 45°$ and negative while the rotor angle is between $\alpha = 135°$ and $\alpha = 165°$.

Diaz et al. [5] analyzed the drag and lift coefficients of a Savonius wind turbine to quantify the aerodynamic performance of the rotor. They found that maximum efficiency, in terms of power coefficient, occurs at a tip-speed ratio of $\lambda = 1$, and the drag coefficient decreases sharply when the tip-speed ratio increases or decreases from this value. They also found that the most important region of Savonius rotor operation occurs at a tip-speed ratio around $\lambda = 1$, where the lift coefficient remains as a constant 0.5.

Sawada et al. [33] studied the mechanism of rotation of a Savonius rotor with two semi-cylindrical blades and found that a rotor with gap ratio of 0.21 produces positive static torque at all angles. They also found that lift force contributes significantly to dynamic torque while the rotor angle is between $\alpha = 240°$ and $\alpha = 330°$.

Aldoss and Obeidat [1] used the discrete vortex method to analyze the performance of two Savonius rotors running side-by-side at different separations. They compared their computational results on torque and power coefficients with their experimental results for verification.

Fujisawa and Gotoh [8] studied the aerodynamic performance of a Savonius rotor by measuring the pressure distributions on the blade surfaces at various rotor angles and tip-speed ratios. They found that the pressure distribution on the rotating rotor differs remarkably from those on the stationary rotor, especially on the convex side of the advancing blade, where a low-pressure region is formed by the moving-wall effect of the blade. Torque and power performance, evaluated by integrating the pressure, were in close agreement with direct torque measurements.

Rahman et al. [26-28] experimentally studied aerodynamic characteristics, such as the torque and drag coefficients, of a three-bladed Savonius rotor model by measuring the pressure

difference between the convex and concave surfaces of each semi-cylindrical blade of the stationary rotor at different rotor angles and the variation of the separation point with the increase of rotor angle. They used the static coefficients for dynamic prediction and compared the findings in terms of power coefficient for different tip-speed ratios with experimental results for the two-bladed Savonius rotor.

Although the starting torque for Savonius rotors is high, it is not uniform at all rotor angles. The torque characteristics of an ordinary Savonius rotor have two problems. First, they vary significantly at different rotor angles, causing the rotor to vibrate and consequently decrease its durability. Second, the torque at the rotor angle ranging from 135° to 165° and from 315° to 345° is negative or very small, which hinders its use as a starter [11]. To decrease this torque variation and improve starting characteristics, a new type of Savonius rotor was designed and fabricated by Hayshi et al. [12]. It had three stages, with a 120° bucket phase shift between adjacent stages. With this design, wind-tunnel tests showed that both static and dynamic torque variations in one revolution were much smoother compared to an ordinary one-stage rotor, which greatly improved the starting characteristics. They also measured the torque characteristics of the rotors with guide vanes and found that, on the average the guide vanes increased the torque coefficient in the low tip-speed ratio but decreased it in the high tip-speed ratio. They concluded that two- and three-stage conventional Savonius rotors could overcome the problem of negative torque. However, the maximum power coefficient decreases for this kind of design with more stages.

To decrease the variation of static torque in conventional Savonius rotors with rotor angle ranging from 0° to 360°, Kamoji and Kedare [15] tested a helical rotor with a twist of 90°. They conducted experiments in an open-jet wind tunnel at gap ratios of 0.0, 0.05, and 0.08 to study the

effect of the overlap ratio and the Reynolds numbers on its performance to evaluate the static torque, the dynamic torque, and the power coefficients. They compared its performance with and without a shaft between the end plates at different overlap ratios. A helical rotor without a shaft was also compared with the performance of the conventional Savonius rotor. They found that all helical rotors have a positive power coefficient of static torque for all rotor angles, but the rotors with a shaft had a lower power coefficient than those without. The power coefficient of the rotor without a shaft with a zero overlap ratio was marginally less than the conventional Savonius rotor. The rotor appeared to be sensitive to the Reynolds number, but this finding must be confirmed by rigorous experiments.

McWilliam and Johnson [18] investigated various Savonius wind turbine models to observe the vortex formation and the effect of the scale of downstream wake using particle image velocimetry (PIV) in a close loop wind tunnel. In that experiment, they used standard Savonius design (diameter = 30.18 mm) with two semicircular blades overlapping. The design of these blades include deep blade design (diameter = 31.20 mm), shallow blade design (diameter = 28.04 mm), outside J blade design (diameter = 32.97 mm) and inside J blade design (diameter = 31.18 mm). They executed the experiment at a constant 3 m/s wind velocity. They observed that vortex shedding from the following blade was common to all five designs they tested, which had an effect on the scale of the downstream wake of the rotor. They found that the forward curved blade was the critical area for external flow and the overlap ratio of Savonius wind turbine blades allows flow from the top blade to enter the bottom blade that reduces the negative pressure region behind the blades.

Saha et al. [30] fabricated a two-stage Savonius wind turbine by inserting valves on the concave side of the blades. They compared its performance with a conventional Savonius wind

turbine and found that with valves on a three-bladed turbine, the power coefficient was higher compared to a two-bladed turbine for both semi-circular and twisted blades. Without valves, air strikes the blades and rotates them in a negative direction. They also varied the number of stages in a Savonius wind turbine and found that the power coefficient increase from a one-stage design to a two-stage design but decrease from a two-stage design to a three-stage design due to increased inertia. They tested twisted blades of one, two, and three-stages and found that three-stage design had a better power coefficient and the twisted-blade design showed better performance.

Gupta et al. [9] compared a three-bucket Savonius wind turbine with a three-bucket Savonius– Darrieus wind turbine. They found that the power coefficient of the combined turbine is decreases as the overlap ratio increases. The maximum power coefficient of 51% was found where there was no overlap. They claimed that the combined rotor without overlap, which showed 51% efficiency, was the highest efficiency of a Savonius wind turbine at any overlap condition under these test conditions.

Altan et al. [3] did some experimental studies to improve the performance of the Savonius wind turbine using curtain. They placed curtain arrangement in front of the rotor in a way that is capable of preventing the negative torque that affects the convex blade surface of the Savonius wind turbine.

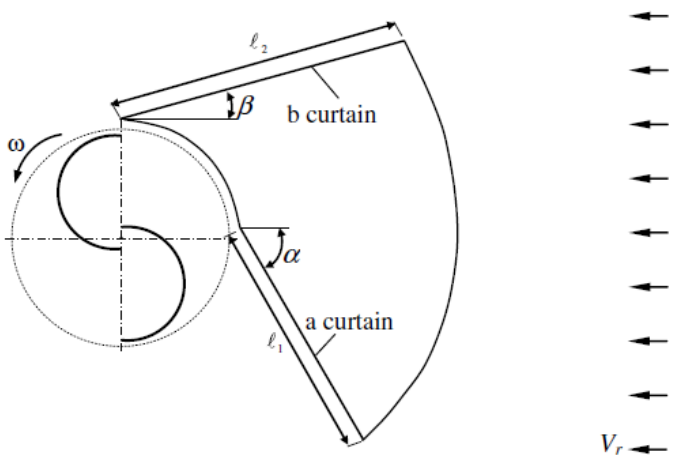

Figure 2.1: Curtain positioning of Altan et al. experiment [3]

They performed the experiment with curtain and without curtain. They found that optimum curtain angle was α = 45° and ß = 45° where they achieved the highest power coefficient. The numerical value for the power coefficient was 38% greater than the design without curtain. Other curtains also showed that the power coefficient can be improved by 16% compared to the design without curtains.

Literature review on Numerical investigation

Benjanirat et al. [4] numerically investigated the performance of the NREL phase VI horizontal axis wind turbine. They used 3D unsteady Navier-Stokes solver and their solver was third order accurate in space and second order accurate in time. They also used an implicit time marching scheme to solve their numerical simulation. They varied their wind speed from 7 m/s to 25 m/s and studied three turbulence models: Baldwind-Lomax model, Spalart-Allmara one equation model and k-ε two equation model with and without wall corrections. From the investigation they found that torque is increased while the wind speed changes from 7 m/s to 10

m/s. The flow was largely attached over the entire blade rotor. The torque is decreased while the wind speed changes from 10 m/s to 20 m/s because of progressive growth of separated flow region. The flow was fully separated above wind speed 20 m/s. In their experiment, the Spalart-Allmara model and the k-ε model without near wall correction showed good prediction for the low speed torque but which did not agree with experimental results. They found that k-ε model with near wall correction was the most accurate prediction.

Lida et al. [17] performed a numerical simulation of vertical axis wind turbine (Darrieus wind turbine) with large eddy simulation (LES) using the sliding mesh technique. Their wind turbine had three straight airfoil type (NACA0018) wings. The dimensions of their design were Diameter: 3600 mm, cord length: 300 mm and span wise length: 240 mm. To solve the large separated unsteady flow, they used incompressible the Navier-Stokes equation and for the turbulence sub grid the scale model was used. They divided their grid in three parts of rotational grid, stationary grid and buffer grid. Their mesh was coarse at the buffer region. They applied uniform inlet wind speed 6 m/s at inlet boundary condition and zero static pressure at outlet boundary condition. There was no slip condition at blades and cylinder surface and symmetric boundary condition for both side of span wise direction. Their tip speed ratio was from 2 to 6. Their large eddy simulated results were in good agreement with conventional momentum theory. They also found the effect of divergence flow and dynamic stall was small at high tip speed ratio and becomes large at low tip speed ratio. They also found that power coefficient is significantly decrease in the high tip speed ratio region and suggested reduce time ratio.

Sargolzaei et al. [31] simulated Savonius wind turbine using artificial neural networks (ANNs) to estimate power ratio and torque. They experimentally investigated seven prototype Savonius wind turbine and compared with their predicted ANNs results. Their predicted results

were in good agreement with their experimental results. They found that the increase of wind speed causes torque increase. For all their models they found maximum torque was at 60° and minimum torque was at 120°.

Altan et al. [2] numerically simulated their experimental work using Fluent 6.0 and Gambit 2.0. Their model was two-dimensional, and they used a standard k-ε turbulence model. To calculate pressure and velocity distribution, they used a SIMPLE analysis algorithm. By comparing the numerical and experimental results, they concluded that the curtain improved the performance of Savonius wind turbines.

CHAPTER 3

METHODOLOGY

Introduction

In this research, aerodynamic characteristics of a three bladed Savonius vertical axis wind turbine (VAWT) with different overlap ratios were investigated using both experimental and numerical methods. The experimental part of this research was conducted in front of an open circuit subsonic wind tunnel. Numerical investigation was performed using commercial software GAMBIT and FLUENT. GAMBIT was used to generate mesh of the flow domain around the three blades of the turbine models; these mesh files were then exported in FLUENT to solve the fluid flow field to determine the aerodynamics coefficients such as torque and power coefficients. This chapter describes in detail the experimental set up design and development, experimental data measurement procedure, design and fabrication of three rotor models, numerical model selection and validation, and numerical technique to solve fluid flow.

Experimental set-up Design and Development

Subsonic Wind Tunnel

A subsonic wind tunnel was designed and fabricated for the experimental part of this research as shown in Figure 3.1. The wind tunnel was designed using solid modeling and fabricated at in-house machine shop. The wind tunnel is 12 feet long which consists of converging mouth entry, honeycomb section 1, test section, fan section, rectangle section, honeycomb section 2, converging diverging section and rectangular exit section.

Figure 3.1: Subsonic wind tunnel

The converging mouth entry section (2 ft long) was incorporated into the system to ease entry of air into the tunnel and to maintain uniform flow through the tunnel. The test section (1 ft long) was made with transparent acrylic sheet. First honeycomb section (0.5 ft) was used to reduce swirling effect and make the flow straight. A single stage axial flow fan was used to induce flow through the wind tunnel. Second honeycomb section (0.5 ft) was used to make flow straight. Converging and diverging section (each section 2.25 ft long) was used to minimize expansion and contraction loss and to reduce the possibility of flow separation. The exit section (2 ft long) and other rectangular section were used to make the flow straight and uniform.

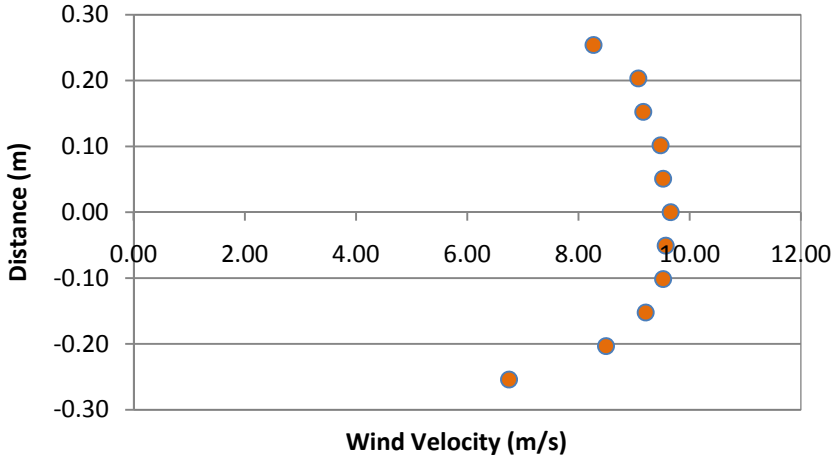

Figure 3.2: Velocity profile at a distance of 89 cm from the wind tunnel outlet.

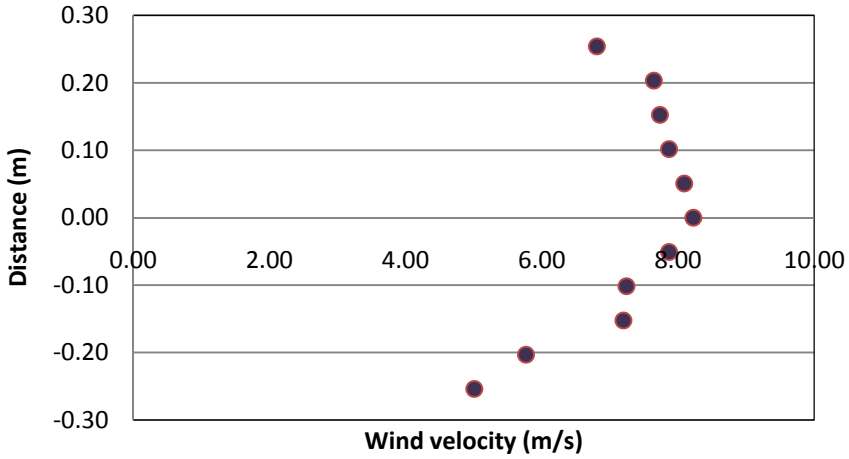

Figure 3.3: Velocity profile at a distance of 300 cm from the wind tunnel outlet.

Wind velocity was measured by traversing an anemometer vertically with every 50 mm vertical position for four different locations in front of the wind tunnel exit. Figures 3.2 and 3.3 show the velocity profiles at a distance of 89 cm and 300 cm from the outlet of the wind tunnel.

Three Bladed Savonius rotor Models

To observe the effect of overlap ratio (ratio between the distance of the two adjacent blades and rotor diameter) and Reynolds number on the aerodynamic characteristics of the Savonius rotor, three different rotor models with and without overlap ratio were designed and physically fabricated. These three models were tested in front of the subsonic wind tunnel for various Reynolds number flow conditions.

Savonius Rotor Model 1

The three bladed Savonius rotor model called Model 1 with no overlap between adjacent blades was designed and fabricated. Top, front, 3D design views and the fabricated scale model of the Savonius wind turbine are shown in Figure 3.4 (a), 3.4(b), 3.4(c) and 3.4(d) respectively. The model was made of three semi-cylindrical blades of diameter, d = 127 mm, and height, H = 300 mm. The turbine model was made of acrylic. The central shaft was removed from the turbine model. The blades were 120° apart from each other and the overall rotor diameter was D = 248 mm for the Model 1.

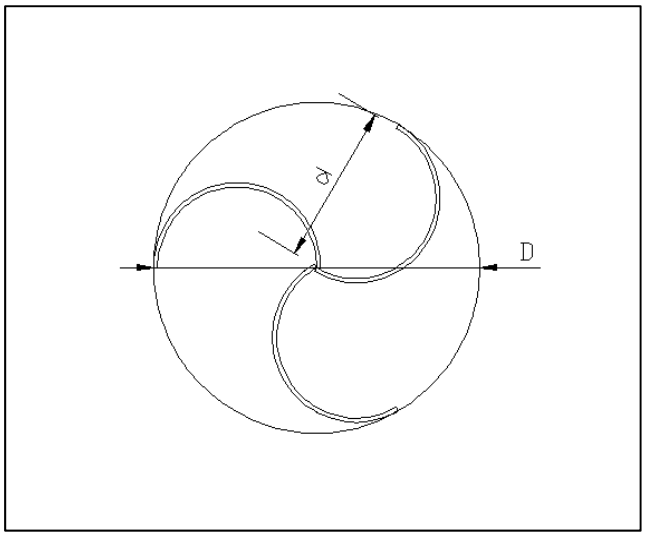

Figure 3.4(a): Top view of Model 1

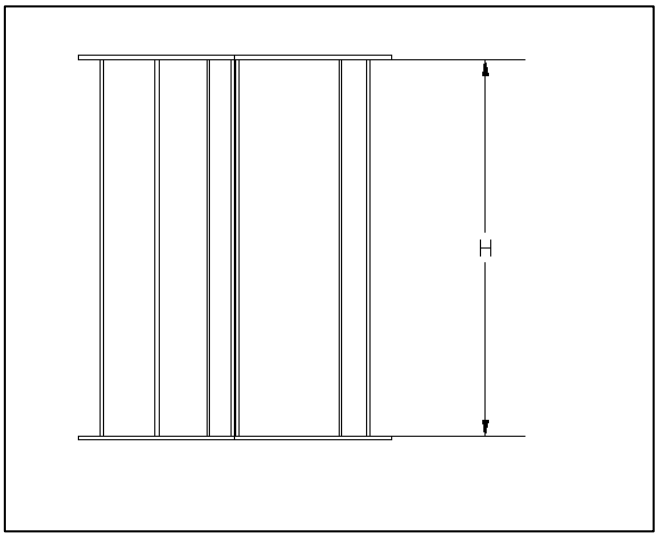

Figure 3.4(b): Front view of Model 1

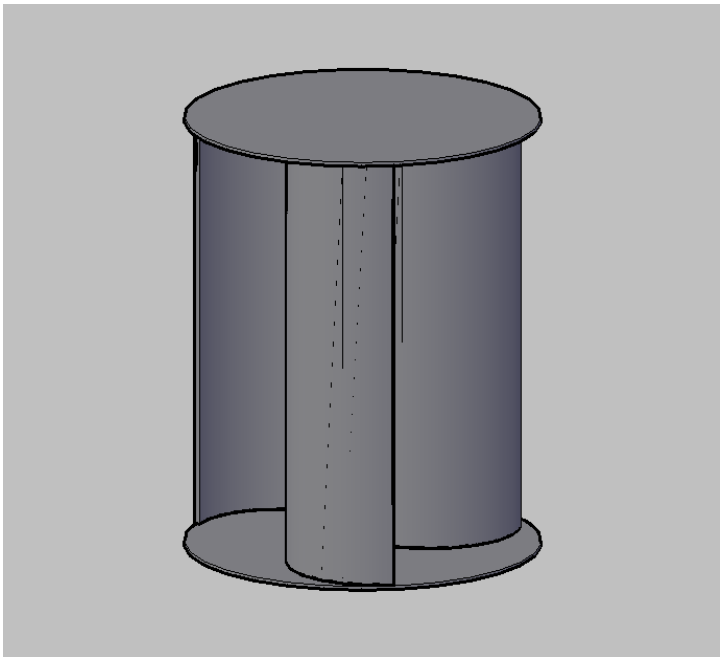

Figure 3.4(c): 3D view of Model 1

Figure 3.4(d): Fabricated Model 1

Savonius Rotor Model 2

Savonius rotor Model 2 with overlap distance between adjacent blades, a = 25 mm, was designed and fabricated. Top, front, 3D design views and the fabricated scale Model 2 of the Savonius wind turbine are shown in Figure 3.5 (a), 3.5(b), 3.5(c) and 3.5(d) respectively. The model was made of three semi-cylindrical blades of diameter, d = 127 mm, and height, H = 300 mm. The turbine model was made of acrylic without any central shaft. The blades were 120° apart from each other and the overall rotor diameter was D = 216 mm for the Model 2. Overlap ratio for Model 2 was 0.12.

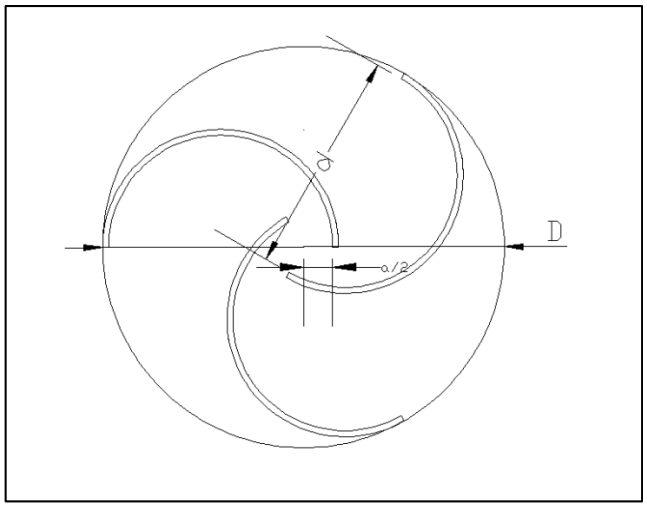

Figure 3.5(a): Top view of Model 2

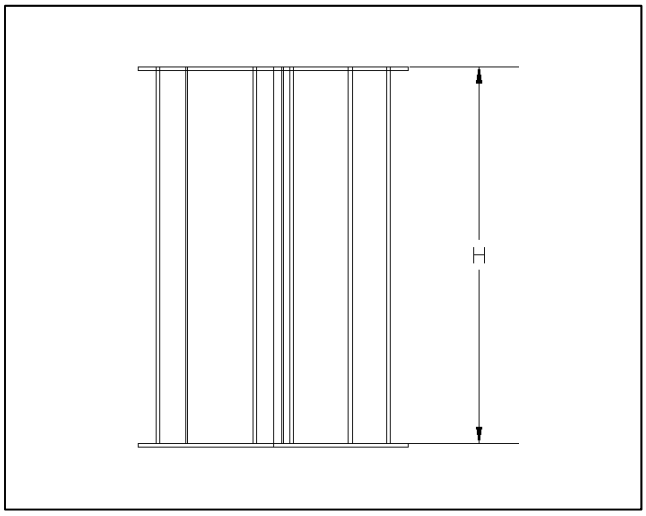

Figure 3.5(b): Front view of Model 2

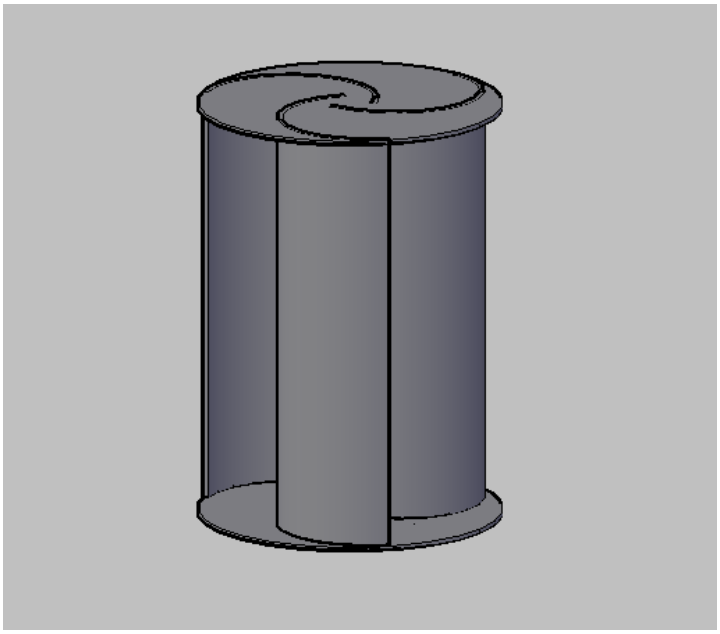

Figure 3.5(c): 3D view of Model 2

Figure 3.5(d): Fabricated Model 2

Savonius Rotor Model 3

Savonius rotor Model 3 with overlap distance between adjacent blades, a = 50 mm, was designed and fabricated. Top, front, 3D design views and the fabricated scale Model 2 of the Savonius wind turbine are shown in Figure 3.6 (a), 3.6(b), 3.6(c) and 3.6(d) respectively. The model was made of three semi-cylindrical blades of diameter, d = 127 mm, and height, H = 300 mm. The turbine model was made of acrylic without any central shaft. The blades were 120° apart from each other and the overall rotor diameter was D = 192 mm for the Model 3. Overlap ratio for Model 3 was 0.26.

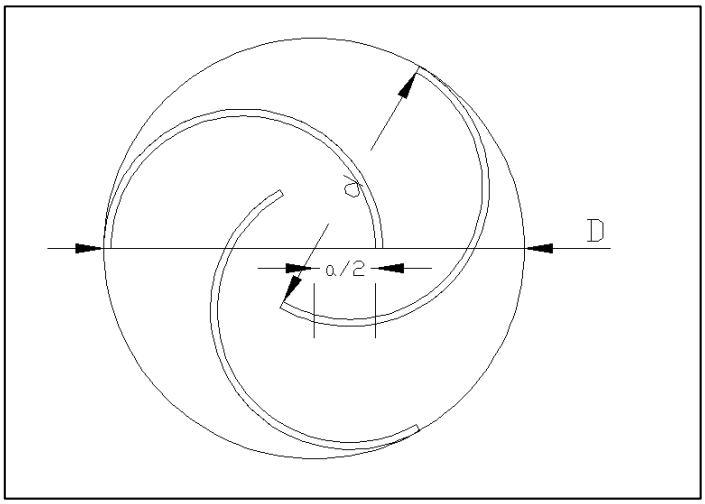

Figure 3.6(a): Top view of Model 3

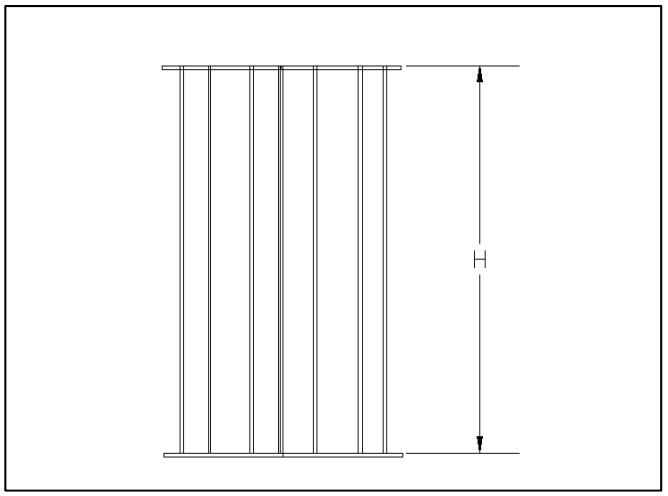

Figure 3.6(b): Front view of Model 3

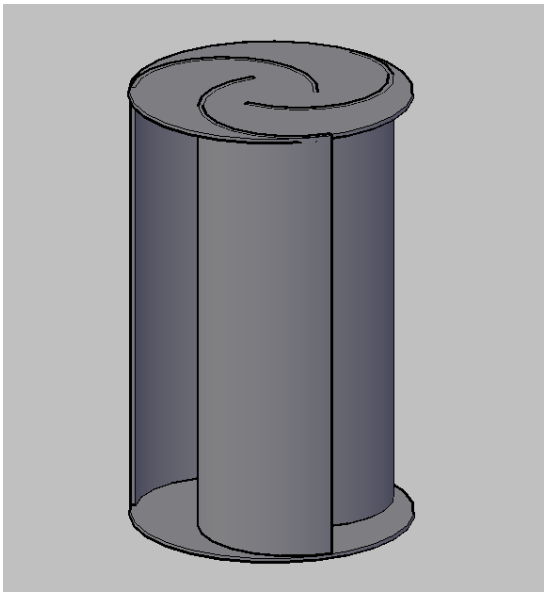

Figure 3.6(c): 3D view of Model 3

Figure 3.6(d): Fabricated Model 3

Mathematical Expressions

Rotor Area: $A = D.H$ [3.1]

Overlap Ratio: $OR = \frac{a}{D}$ [3.2]

Aspect Ratio: $AR = \frac{H}{d}$ [3.3]

Angular Velocity: $\omega = \frac{2\pi N}{60}$ [3.4]

Reynolds Number:$Re = \frac{VD}{\nu}$ [3.5]

Tip Speed Ratio: $\lambda = \frac{\omega D}{2V}$ [3.6]

Torque Coefficient: $C_q = \frac{T}{\frac{1}{4}\rho A D V^2}$ [3.7]

Power Coefficient: $C_p = \frac{P}{\frac{1}{2}\rho A V^3} = \frac{T\omega}{\frac{1}{2}\rho A V^3}$ [3.8]

Normal Drag Force: $F_n = \int_0^{\pi} \Delta p \frac{d}{2} cos\emptyset d\emptyset = \sum_{i=1}^{17} \Delta p_i \frac{d}{2} cos\emptyset_i \Delta\emptyset_i$ [3.9]

Tangential Drag Force: $F_t = \int_0^{\pi} \Delta p \frac{d}{2} sin\emptyset d\emptyset = \sum_{i=1}^{17} \Delta p_i \frac{d}{2} sin\emptyset_i \Delta\emptyset_i$ [3.10]

Normal Drag Coefficient: $C_n = \frac{F_n}{\frac{1}{2}\rho V^2 A}$ [3.11]

Tangential Drag Coefficient: $C_t = \frac{F_t}{\frac{1}{2}\rho V^2 A}$ [3.12]

Lift Coefficient: $C_l = \frac{F_L}{\frac{1}{2}\rho V^2 A}$ [3.13]

Experimental Procedure

Drag Force Measurement

Figure 3.7: A three bladed Savonius rotor Model for pressure measurement.

The pressure distribution around the concave and convex surfaces of each blade were measured experimentally using a semi-cylindrical three bladed Savonius VAWT model with overlap distance, a = 25, between the adjacent blades as shown in Figure 3.7. The rotor model was made of stainless steel material with each blade diameter, d = 125 mm, height, H = 300 mm

and rotor diameter, D =225 mm. The overlap ratio OR was 0.11 (i.e., OR = a/D) and there is no shaft in the rotor model. The whole rotor was mounted on an iron frame using two separate shafts and bearings at the two ends. The convex and concave surface pressures of each blade were measured at 17 tapping points using 1.5 mm outer diameter and 10 mm length copper tubes which were press fitted to 17 tapping holes. These tapping points were located at the mid-plane of each blade to measure the pressure at every 10° interval on the blade surface. The copper tubes were connected to 17 pressure transducers PX277 through 2 mm PVC tubes. Pressures were measured at every 30° interval of rotor angle. A personal computer equipped with data acquisition system was used to record and edit the pressure data. Average wind speed during this experiment was 9.61 m/s. Reynolds number based on rotor diameter was 1.47×10^5. The effect of temperature was considered in this measurement technique which was carried out at atmospheric temperature. The normal and tangential drag forces on each blade of the Savonius rotor model were calculated using the measured pressure difference between the concave and convex surfaces of the blades using equations 3.9 and 3.10. Figure 3.9 shows the cross-section of the rotor with the normal and tangential drag forces direction. Next, tangential and normal drag coefficient was calculated using equations 3.11 and 3.12.

Static Torque Measurement

The experiment was carried out at three different wind speeds V = 9.66 m/s, 8.23 m/s and 7.33 m/s,. The Reynolds numbers based on the rotor diameter varied from 9.94×10^4 to 1.6×10^5. Experiments were carried out and data was recorded at room temperature. Static torque (T) for the three different models of the Savonius wind turbine was measured using a static torque meter (Model: TQ-8800) at three different wind speeds. Torque meter output was in LB-inch which

was then converted into N-m. Rotational speed (N) was measured using a non contact photo tachometer. Equation 3.4 was used to calculate the angular velocity from the rotational speed.

Figure 3.8: Experimental setup of wind tunnel and Savonius rotor model for static torque measurement.

Savonius wind turbine is drag type VAWT where the lift forces are considered to be negligible. Figure 3.8 shows the experimental setup for torque measurement of a Savonius wind turbine model. When the wind strikes the blade surfaces of the model, two components of drag force are generated on each blade surface. Normal drag force (F_N) acts perpendicular on the blade surface and tangential drag force (F_T) acts along tangential direction on each blade. Figure 3.9 shows the schematic diagram of the Savonius rotor cross-section with the components of drag forces on each blade. The pressure difference between the concave and convex surfaces on each blade produces these tangential and normal drag forces. These components of drag forces are

responsible for torque generation within the turbine shaft which can be measured using a torque meter. Equation 3.7 is used to calculate the torque coefficient from the measured torque value. Power coefficient can be calculated from the measured torque and angular velocity of the rotor *using equation 3.9.*

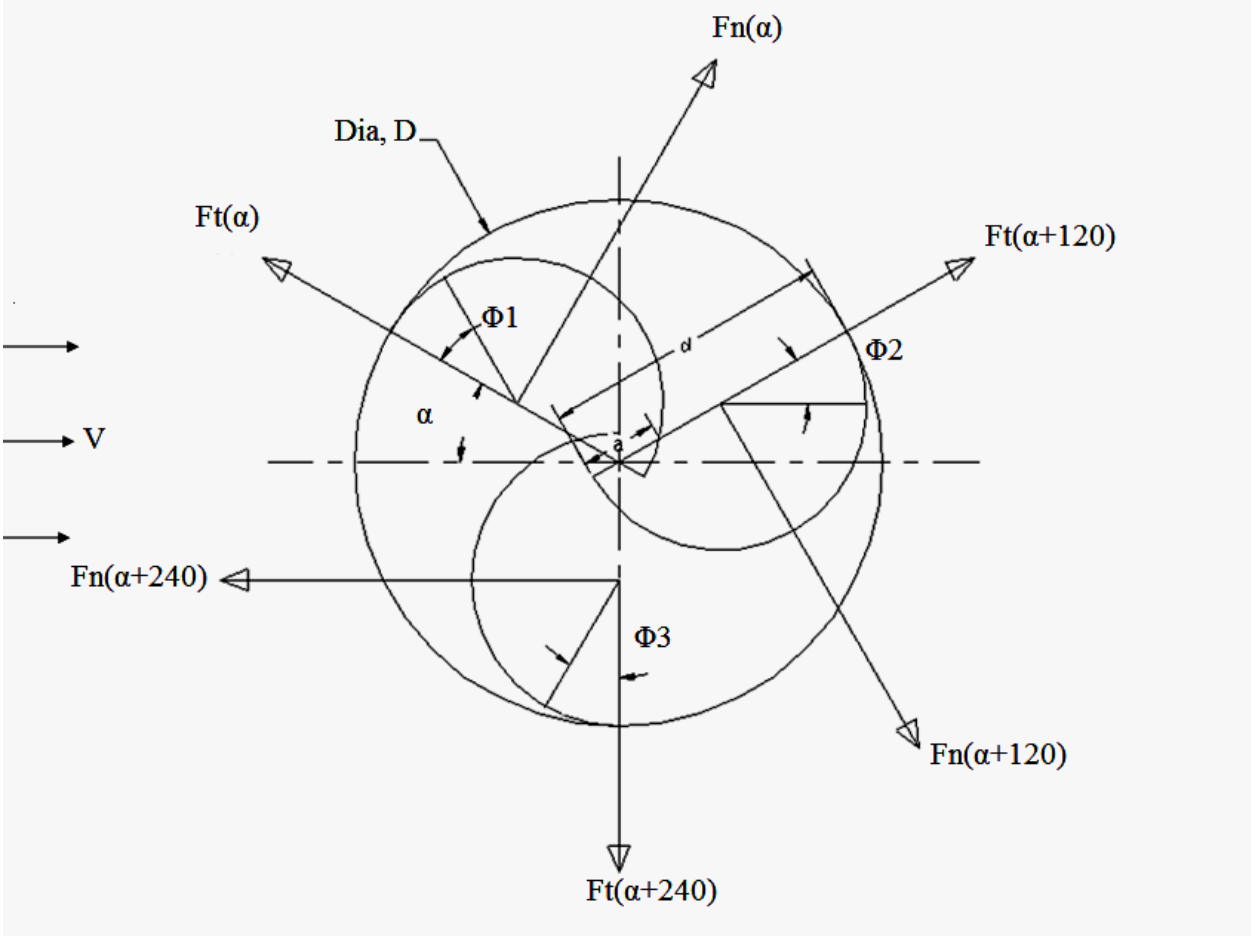

Figure 3.9: Schematic diagram of the rotor model cross-section showing the normal and tangential drag forces on each blade.

Selection of Numerical Model

For the selection of the numerical model from the Computational Fluid Dynamics (CFD) code FLUENT 2D, a NACA 4412 airfoil was numerically examined at the different angle of attack and compared with established research results. For 2D modeling a mesh was generated around the airfoil using GAMBIT. Total of 12,451 nodes were generated and clustering was imposed near the boundary of the airfoil where the mesh was relatively coarser. Figure 3.10 shows the mesh around the airfoil after exported to FLUENT.

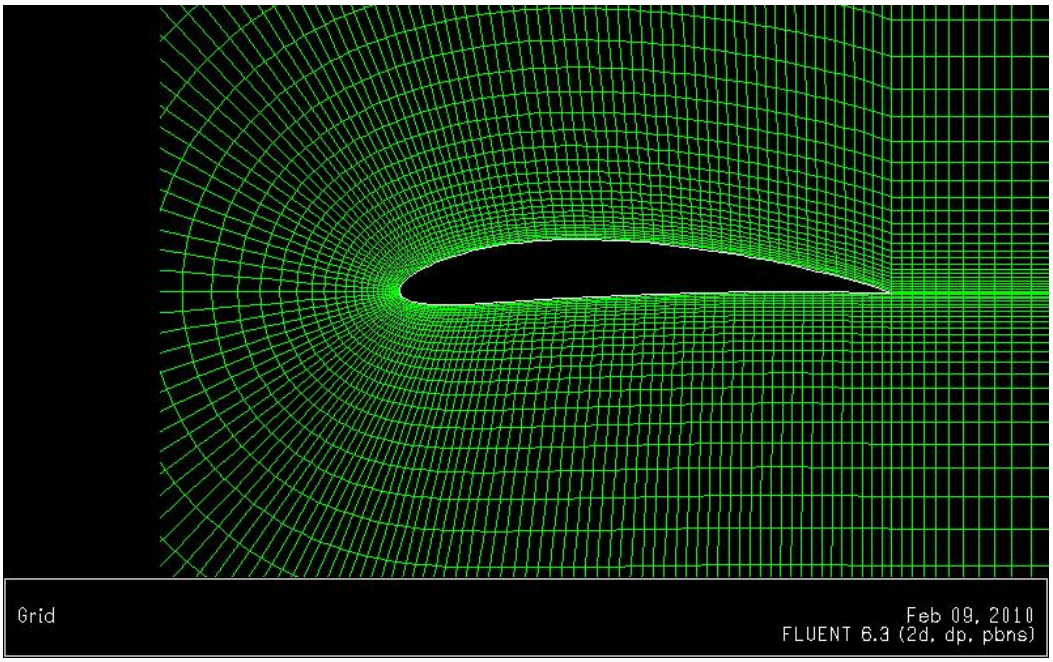

Figure 3.10: Mesh around the NACA 4412 airfoil using FLUENT.

The numerical testing of the airfoil was conducted using the same ambient and fluid flow condition as was used by the previous research for verification. These conditions are wind speed, V = 45.48 m/s, Reynolds number, Re = 3,000,000, air density, ρ = 1.225 kg/m^3, air viscosity, μ = 1.8571×10^{-5}, operating pressure P = 101325 Pa. Investigation was performed for three different angles of attack 2°, 4° and 8°. Investigation was carried out using two different numerical models

such as inviscid model and standard k-ε two equation turbulence model with the enhance wall treatment options. Inviscid flow is suitable for higher Reynolds number where the effect of viscosity is negligible and where initial force is dominating over viscous force. So inviscid flow is very appropriate for aerodynamic analysis where this type of analysis will give a quick estimation of drag and lift forces action on the body surface [6]. Since the k-ε turbulence model was proposed by Launder and Spalding in 1972 [16], it became popular for its robustness and accuracy for a wide range of turbulence flow. The standard k-ε model is a semi-empirical model which is based on model transport equations for turbulence kinetic energy k and dissipation rate ε [6].

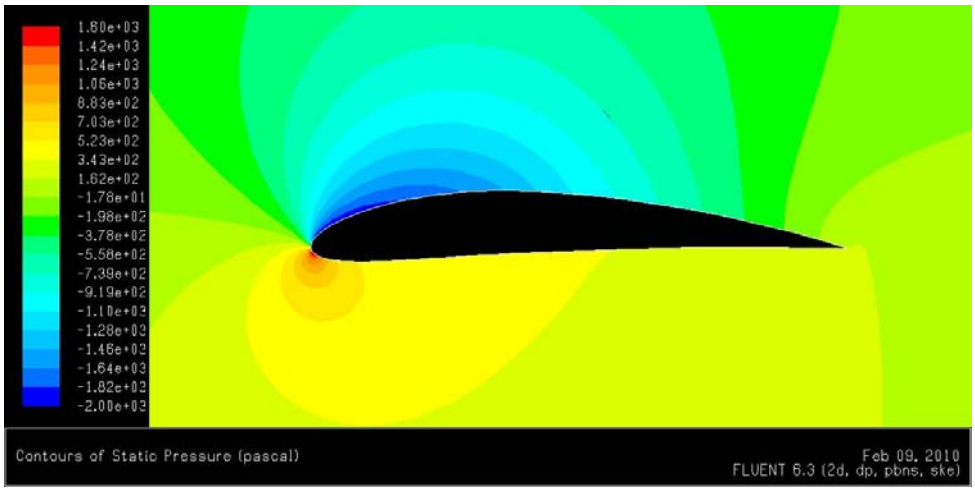

Figure 3.11: Pressure Contours around the airfoil model at 2° angle of attack (Inviscid flow)

Figures 3.11 show the pressure contours generated at 2° angle of attack using the inviscid model. Low pressure zone was established at the middle of the airfoil for the angle of attack 2° then it propagated towards the leading edge of the airfoil with the increase of the angle of attack. Similar pattern was observed for the velocity counters where the higher velocity zone propagated

towards the leading edge with the increase of the angle of attack. Figures 3.12 and 3.16 show velocity contours and velocity vectors for Inviscid flow at 2° angle of attack.

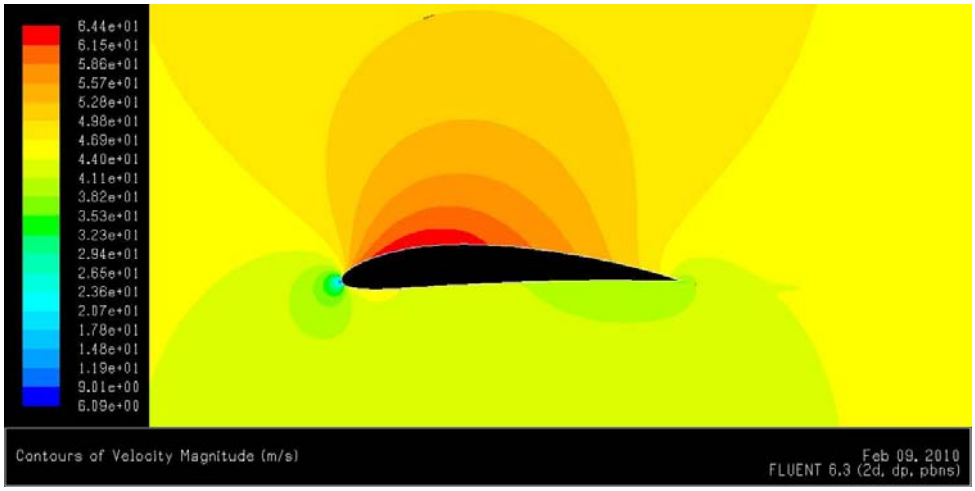

Figure 3.12: Velocity Contours around the airfoil model at 2° angle of attack (Inviscid flow)

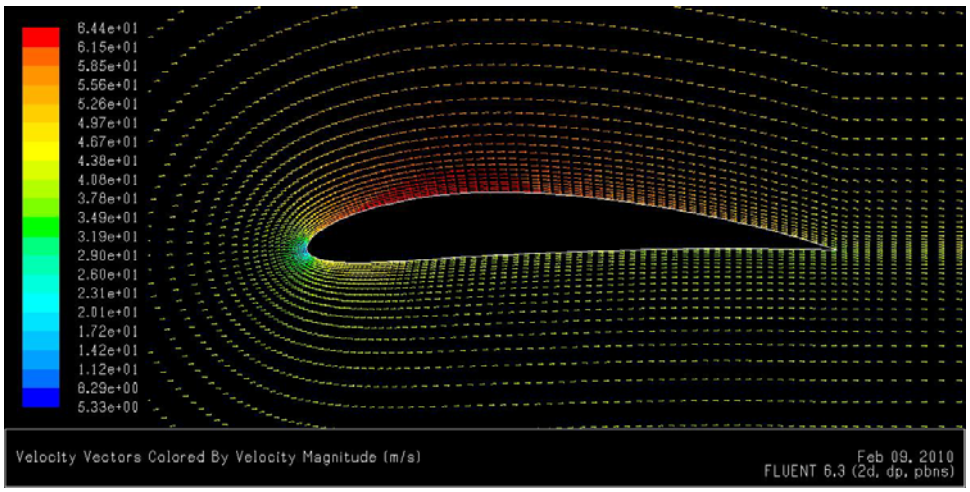

Figure 3.13: Velocity vectors around the airfoil model at 2° angle of attack (Inviscid flow)

Using the flow simulation results from both the inviscid model and the k-ε turbulence model lift coefficient was calculated using equation 3.13 and then compared with published [25] NACA 4412 airfoil results. Table 3.1 shows the comparison of the lift coefficient values calculated using those two models and previous research. Figure 3.14 also shows the graphical comparison of the lift coefficient values from these three different sources. After comparing the inviscid model and the k-ε turbulence model results with established published results it was found that the k-ε turbulence model gave more accurate results than the inviscid model. Therefore, the k-ε turbulence model has been selected for the numerical modeling of the Savonius wind turbine.

Table 3.1:

Lift Coefficient Comparison

Angle of Attack (°)	**Lift coefficient (Inviscid Model)**	**Lift coefficient (k-ε Model)**	**Lift coefficient (Report 563)**[25]
2	0.788	0.678	0.501
4	0.990	0.846	0.667
8	1.404	1.156	1.024

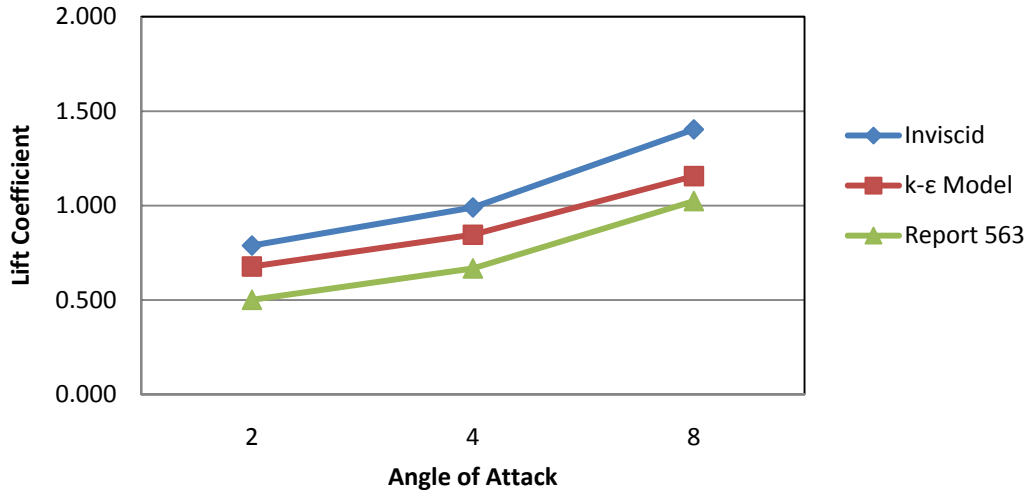

Figure 3.14: Comparison of NACA 4412 airfoil lift coefficient using two numerical models and the previous established model

Numerical Procedure

The k-ε turbulence model was used for the computational flow simulation around the Savonius rotor models with different overlap ratios. Commercially available software FLUENT was used to solve the turbulent flow field and GAMBIT was used for mesh generation around the rotor models. Numerical simulation provides the pressure and velocity values at all nodal points of flow domain around the rotating blades. The purpose of this analysis was to observe the performance of various Savonius VAWTs configurations; it was felt that a 2-D simulation was sufficient for this application. Figures 3.15, 3.16, 3.17 show 2-D mesh generated within a computational domain around three bladed Savonius wind turbine models using GAMBIT in which the position of the three blades were 0°, 120° and 240°. The size of the computational domain was 1.6 m × 1.4 m and the total number of nodes was around 39992. A size function was introduced with the rotor blade to get the better computational results adjacent to the blade

surface. To introduce this size function the minimum mesh size near the blade surface was chosen 0.0005 m × 0.0005 m with the growth rate of 1.1 and maximum mesh size was 0.008 m × 0.008m. In this study triangular mesh was chosen over quadrilateral mesh to reduce the computational time. These generated meshes were then exported in FLUENT for post processing. The flow of air within the domain around the rotor model was assumed to be turbulent and the effects of molecular viscosity were considered negligible. The simplest "complete models" of turbulence are two-equation models in which the solution of two separate transport equations allows the turbulent velocity and length scales to be independently determined.

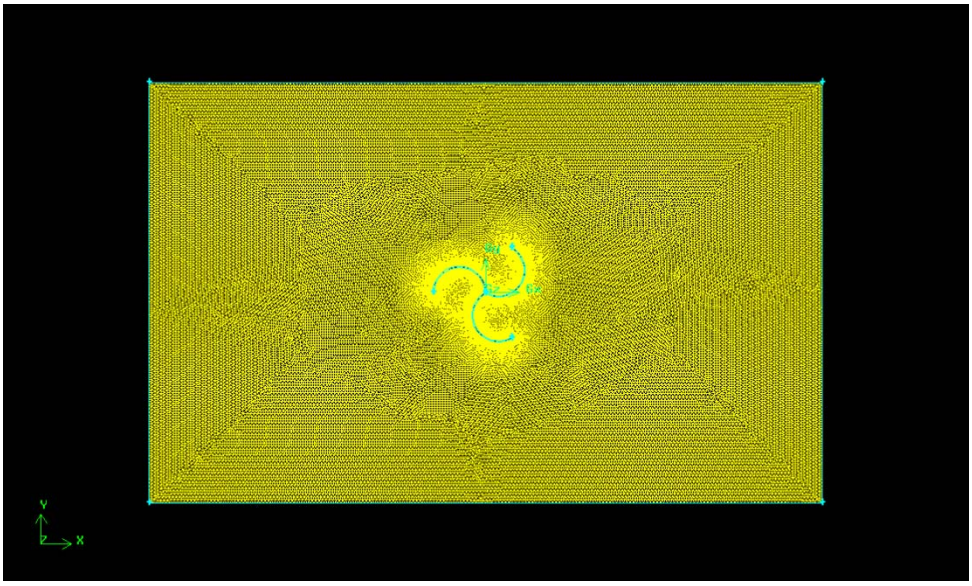

Figure 3.15: Generated mesh using Gambit for Model 1.

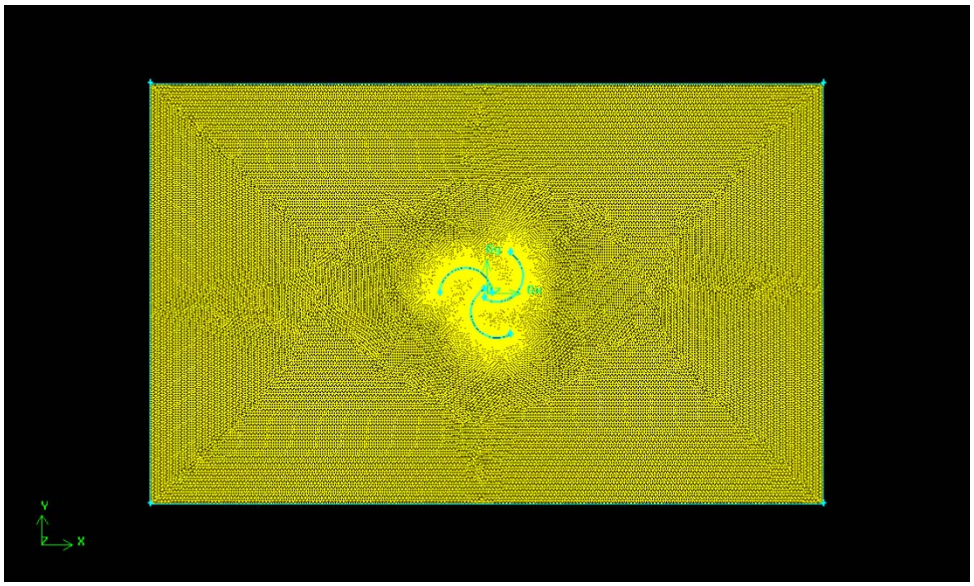

Figure 3.16: Generated mesh using Gambit for Model 2.

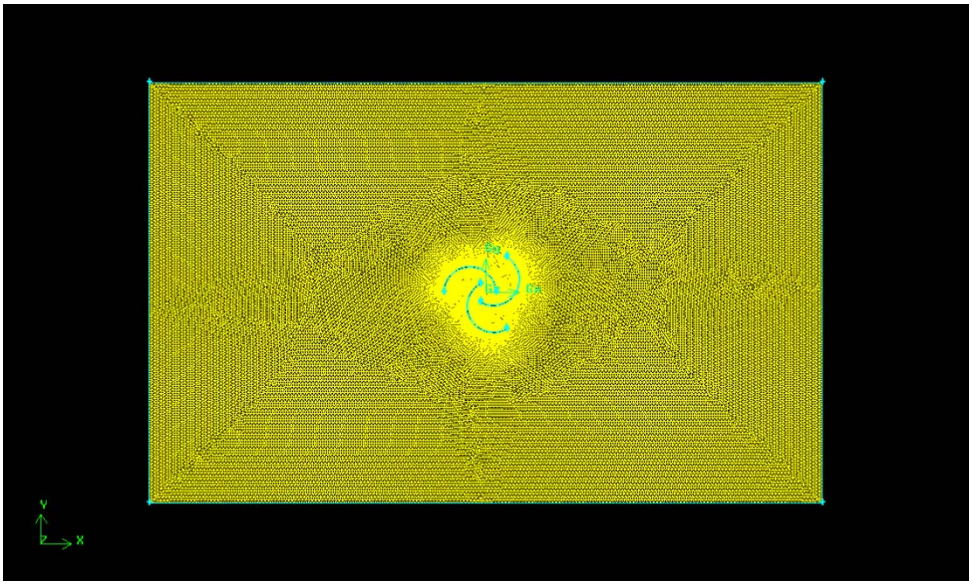

Figure 3.17: Generated mesh using Gambit for Model 3.

The standard k -ε turbulence model in FLUENT was used for the analysis of turbulent flow around rotor models. The pressure-velocity coupling is achieved using the well-known SIMPLE (Semi-Implicit Method for Pressure-Linked Equations) method by Patankar [22]. Turbulent kinetic energy (k) and turbulent dissipation rate (ε) first order upwind scheme was chosen for the momentum equation solution. The standard k-ε turbulence model [16] is a semi-

empirical model based on model transport equations for the turbulence kinetic energy (k) and its dissipation rate (ε). The model transport equation for k was derived from the exact equation, while the model transport equation for (ε) was obtained using physical reasoning and bears little resemblance to its mathematically exact counterpart.

The turbulence kinetic energy, k, and its rate of dissipation, ε, were obtained from the following transport equations:

$$\frac{\partial}{\partial t}(\rho k) + \frac{\partial}{\partial x_i}(\rho k u_i) = \frac{\partial}{\partial x_j}\left[\left(\mu + \frac{\mu_t}{\sigma_k}\right)\frac{\partial k}{\partial x_j}\right] + G_k + G_h - \rho\varepsilon - Y_M + S_k \qquad [3.14]$$

$$\frac{\partial}{\partial t}(\rho \varepsilon) + \frac{\partial}{\partial x_i}(\rho \varepsilon u_i) = \frac{\partial}{\partial x_j}\left[\left(\mu + \frac{\mu_t}{\sigma_\varepsilon}\right)\frac{\partial \varepsilon}{\partial x_j}\right] + c_{1\varepsilon}\frac{\varepsilon}{k}(G_k + C_{3\varepsilon}G_b) - C_{2\varepsilon}\rho\frac{\varepsilon^2}{k} + S_\varepsilon \qquad [3.15]$$

In these equations, G_k represents the generation of turbulence kinetic energy due to the mean velocity gradients, G_b is the generation of turbulence kinetic energy due to buoyancy, Y_M represents the contribution of the fluctuating dilatation in compressible turbulence to the overall dissipation rate, $C_{1\varepsilon}$, $C_{2\varepsilon}$ and $C_{3\varepsilon}$ are constants. σ_K and σ_ε are the turbulent Prandtl numbers for k and ε respectively. S_k and S_ε are user-defined source terms. The turbulent (or eddy) viscosity, μ_t, is computed by combining k and ε as follows:

$$\mu_t = \rho C_\mu \frac{k^2}{\varepsilon} \qquad [3.16]$$

where C_μ is a constant.

Boundary conditions were assigned top and bottom as symmetry, the left side is open with inlet free stream velocity, and the right side is open with an atmospheric pressure outlet. Inlet air velocity was considered the same as experimental value i.e. 9.66 m/s, 8.23 m/s, and 7.33

m/s, air density was considered 1.2 kg/m^3. The blades were considered as moving walls and their rotational velocity was provided from the rpm measured during the experiment. The convergence of the sequential iterative solution is achieved when the sum of the absolute differences of the solution variables between two successive iterations falls below a pre-specified small number, which was chosen as 1×10^{-5} in this study. For all Models using k-ε turbulence model convergence criteria(1×10^{-5}) was set and tested for continuity, x-velocity, y-velocity, kinetic energy (k) and turbulent dissipation rate (ε). It was found that for Model 1 at wind speed 9.66 m/s solution converged at 4019 iterations shown in Figure 3.18. For Model 2 and Model 3 at the wind speed 9.66 m/s solution converged respectively at 1844 and 1307 iterations.

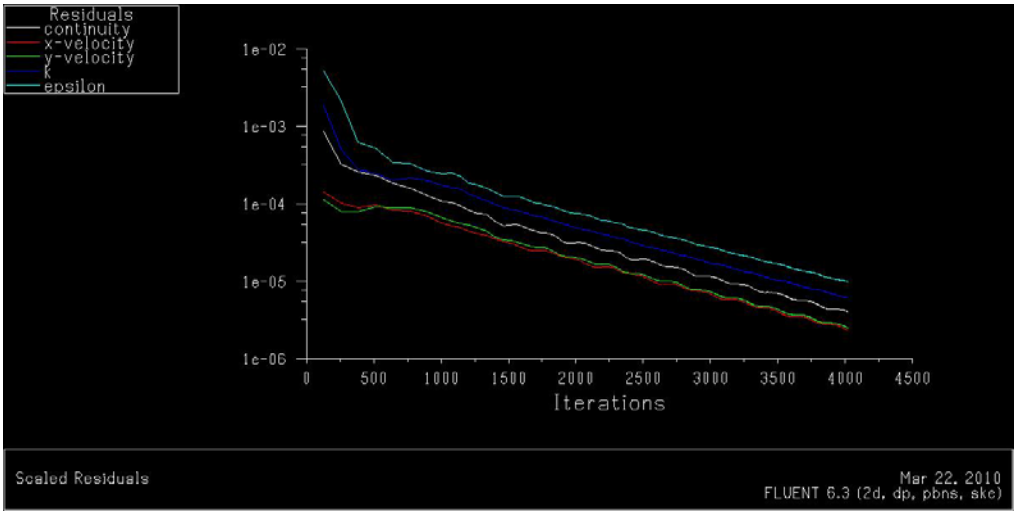

Figure 3.18: Residuals Convergence of Model 1 at wind speed 9.66 m/s.

CHAPTER 4

FINDINGS OF THE STUDY

Introduction

Experimental results of normal drag coefficient, tangential drag coefficient, torque coefficient, and power coefficient of three bladed Savonius VAWTs models with various overlap ratios are discussed in this chapter. The second part of this chapter will discuss the numerical findings of the present study as well as the comparison of torque and power coefficients with the experimental results. Both numerical and experimental investigations were carried out at different wind speed for different Reynolds number.

Experimental Results

Normal and Tangential Drag Coefficient

Normal drag coefficient (C_n) variation with the change in rotor angle (θ) for three bladed Savonius wind turbine model is shown in Figure 4.1. Combined blade effect at 10° interval from 0° to 360° is shown in this plot. Normal drag coefficient increases with the increase of rotor angle from 0° to 60°, and then decreases with the increase of rotor angle up to 100°. Normal drag coefficient is responsible for torque generation in the rotor model. Figure 4.1 also shows that this combined normal drag coefficient remains positive for rotor angle changing from 0° to 90° with its maximum value at 60° which is favorable for torque production. The same pattern of normal drag coefficient repeats from 120° to 230° and from 240° to 350°.

Tangential drag coefficient (C_t) with change in rotor angle (θ) with 10° interval from 0° to 360° is shown in Figure 4.2. Figure also shows that a sharp drop occurs from 0° to 10° and then sharp increase occurs from 10° to 40°. Again a sharp drop occurs in the drag coefficient from 40° to 90° and a sharp increase occurs from 90° to 120°. Results show that tangential drag coefficient remains positive with every angle of rotation this positive value is very important factor for producing thrust in the rotor model. The same pattern of tangential drag coefficient repeats from 120° to 230° and from 240° to 350°.

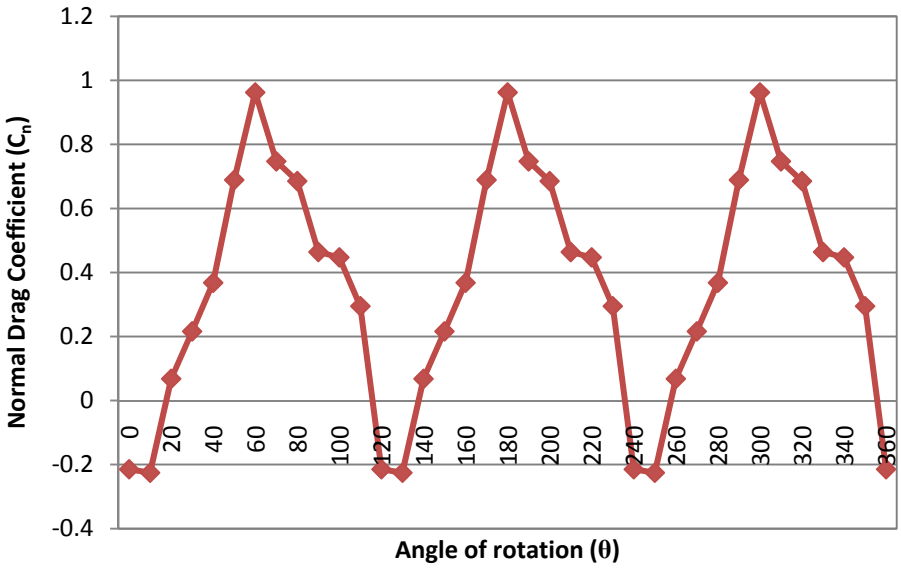

Figure 4.1: Normal Drag Coefficient (C_n) versus Angle of rotation (θ) for three blades combined effect.

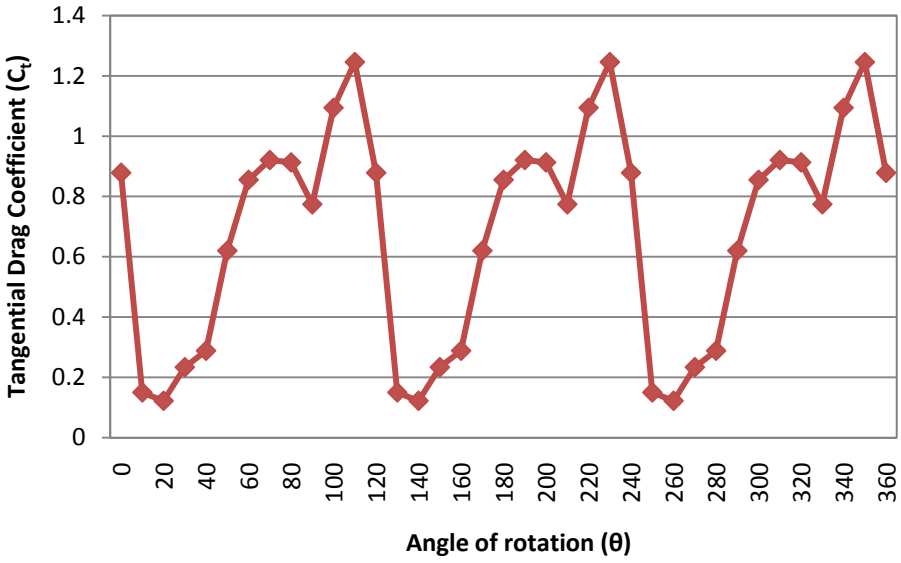

Figure 4.2: Tangential Drag Coefficient (C_t) versus Angle of Rotation (θ) for three blades combined effect.

Torque Coefficient

Torque Coefficient Variation for Three Individual Savonius VAWT Models:

Torque coefficient of Savonius wind turbine ***Model 1*** was calculated for three different Reynolds number. Figure 4.3 shows torque coefficient (C_q) variation with the increase of angle of rotation (θ). Torque coefficient was calculated for combined blade effect at every 30° interval from 0° to 360°. Three Reynolds numbers for Model 1 were 1.61×10^5 (for wind speed 9.66 m/s), 1.37×10^5 (for wind speed 8.23 m/s), and 1.22×10^5 (for wind speed 7.33 m/s). For every Reynolds number the values of torque coefficient increase from 0° to 60° and then start to decrease from 60° to 120°. The same pattern repeats for the blade angle from 120° to 210° and from 240° to 330°. For Reynolds number 1.00×10^5, the value of torque coefficient is negative at

120°, 210° and 240°. It is desired to remove the negative torque for all rotor position , as this negative torque causes reverse rotation which can reduce power output. Figure 4.4 shows torque coefficient (C_q) variation with the angle of rotation (θ) for ***Model 2***. Similarly combined blade effect on torque coefficient with 30° interval from 0° to 360° was calculated. Reynolds numbers for Model 2 were 1.40×10^5 (for wind speed 9.66 m/s), 1.19×10^5 (for wind speed 8.23 m/s), and 1.06×10^5 (for wind speed 7.33 m/s). From the figure it can be seen that the torque coefficient increases from 0° to 60° and decreases at 90° again increases at 120° (except at Re = 1.06×10^5). There was no negative torque coefficient for this model. The same pattern repeats for the blade angel from 120° to 210° and from 240° to 330°. Figure 4.5 shows torque coefficient (C_q) variation with the increase of angle of rotation (θ) for ***Model 3***. Likewise other two models, combined blade effect on torque coefficient at every 30° interval from 0° to 360° was calculated. Reynolds numbers for Model 3 was 1.24×10^5 (for wind speed 9.66 m/s), 1.06×10^5 (for wind speed 8.23 m/s) and 9.44×10^5 (for wind speed 7.33 m/s. For Re = 1.24×10^5, 1.06×10^5 and 9.44×10^5 the pattern of the graph looks similar. Torque coefficient increases from 0° to 60° then decrease at 90° and again increase at 120° (except for Re = 1.24×10^5) . The same pattern repeats for the blade angel from 120° to 210° and from 240° to 330°.

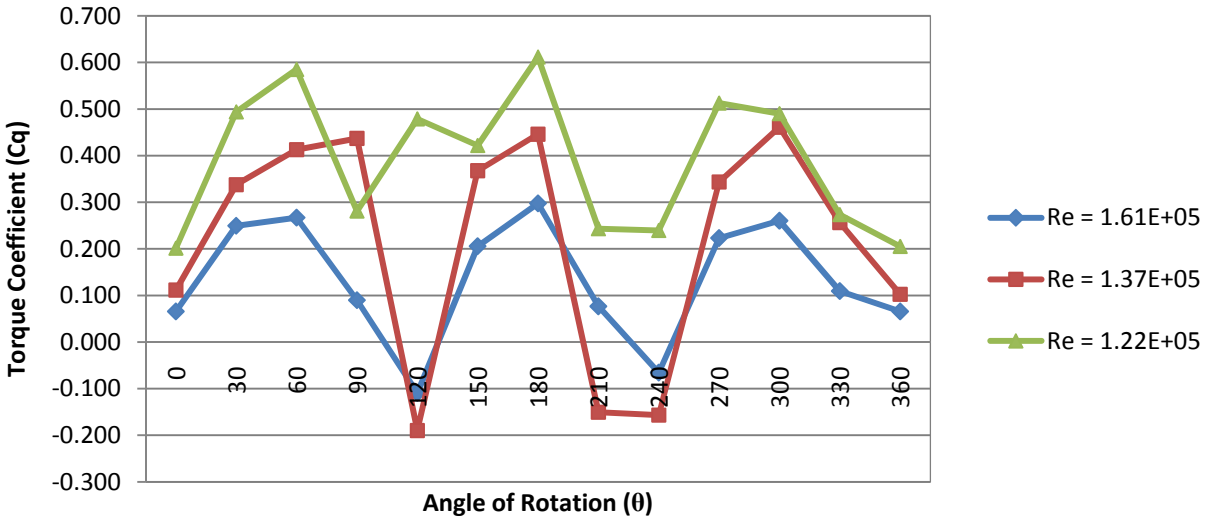

Figure 4.3: Torque Coefficient (C_q) versus Angle of Rotation (θ) for ***Model 1***.

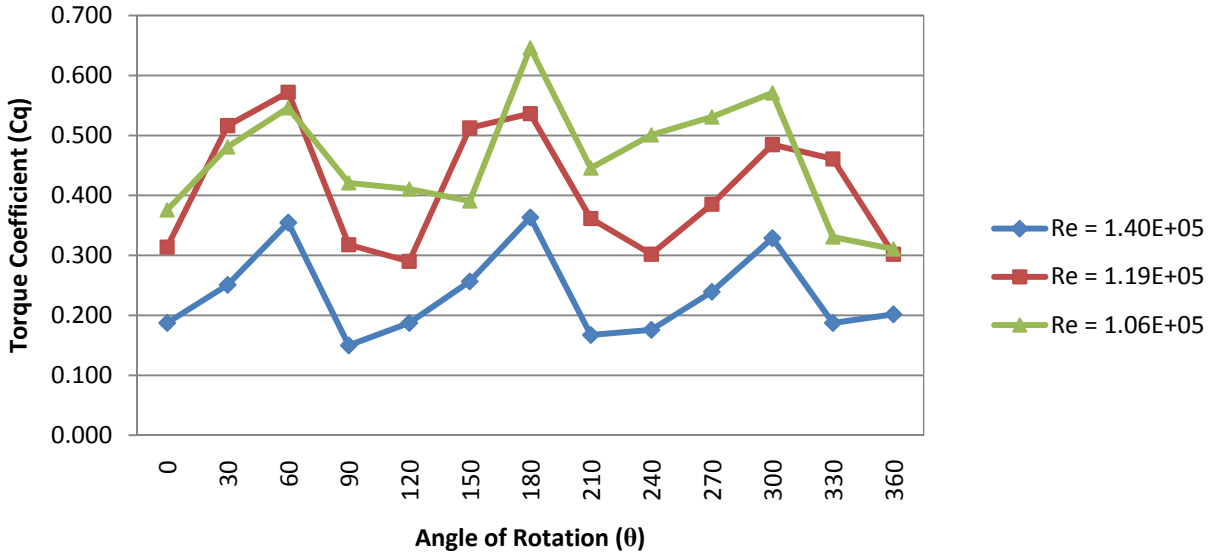

Figure 4.4: Torque Coefficient (C_q) versus Angle of Rotation (θ) for ***Model 2***.

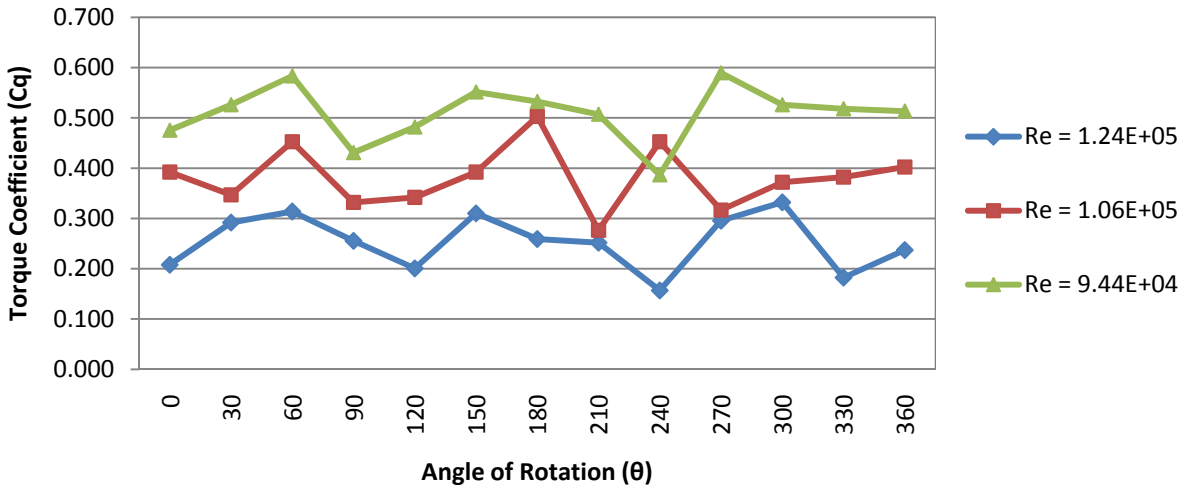

Figure 4.5: Torque Coefficient (C_q) versus Angle of Rotation (θ) for ***Model 3***.

Torque Coefficient Variation at Three Different Wind Speeds:

Torque coefficient (C_q) variation with the angle of rotation (θ) for three models at a wind speed of 9.66 m/s is shown in Figure 4.6. Reynolds numbers 1.61×10^5, 1.40×10^5, and 1.24×10^5 were used for three models respectively with a 30° interval from 0° to 360°. Patterns of the graph for all three models is similar; torque coefficient increases from 0° to 60° and decreases from 60° to 120° (except for model 2). The similar patterns repeat from 120° to 210° and from 240° to 330°. Model 1 exhibits negative torque coefficient at 120° and 240°. Figure 4.7 shows torque coefficient variation with the angle of rotation for three different models at wind speed of 8.23 m/s. Reynolds numbers 1.37×10^5, 1.19×10^5, and 1.06×10^5 were used for Model 1, Model 2 and Model 3 respectively. Figure 4.7 also shows that torque coefficient increases from 0° to 60° and then decreases from 90° to 120° (except for model 1which keeps on increasing till 90°). The same patterns repeat from 120° to 230° and from 240° to 330°. Negative torque coefficient is

observed at 120°, 210° and 240° in Model 1. Figures 4.8 show the torque coefficient variation with the angle of rotation for three different models at wind speed of 7.33 m/s. The pattern of the plot is similar to the previous plots. From these three figures it can be concluded that with the increase of wind speed the corresponding values of torque coefficients decrease as the wind speed increases.

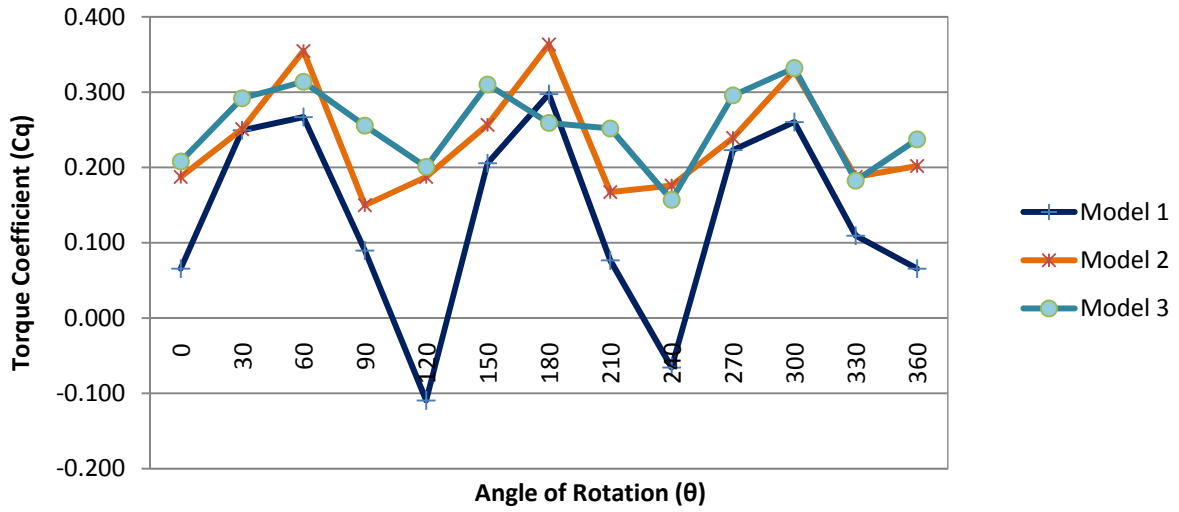

Figure 4.6: Torque Coefficient (C_q) versus Angle of Rotation (θ) at ***wind speed of 9.66 m/s***.

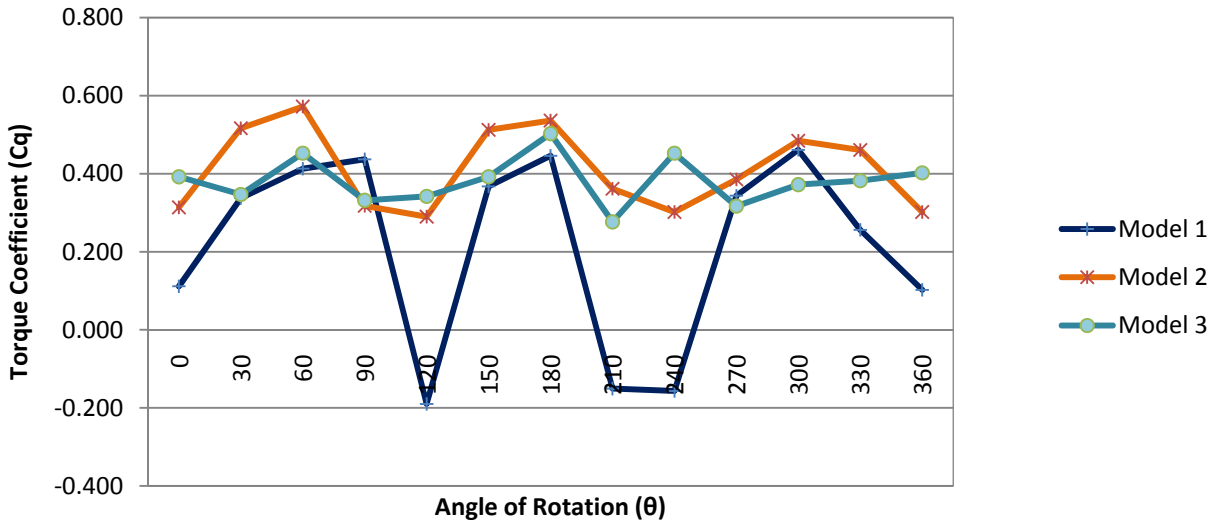

Figure 4.7: Torque Coefficient (C_q) versus Angle of Rotation (θ) at ***wind speed of 8.23 m/s***.

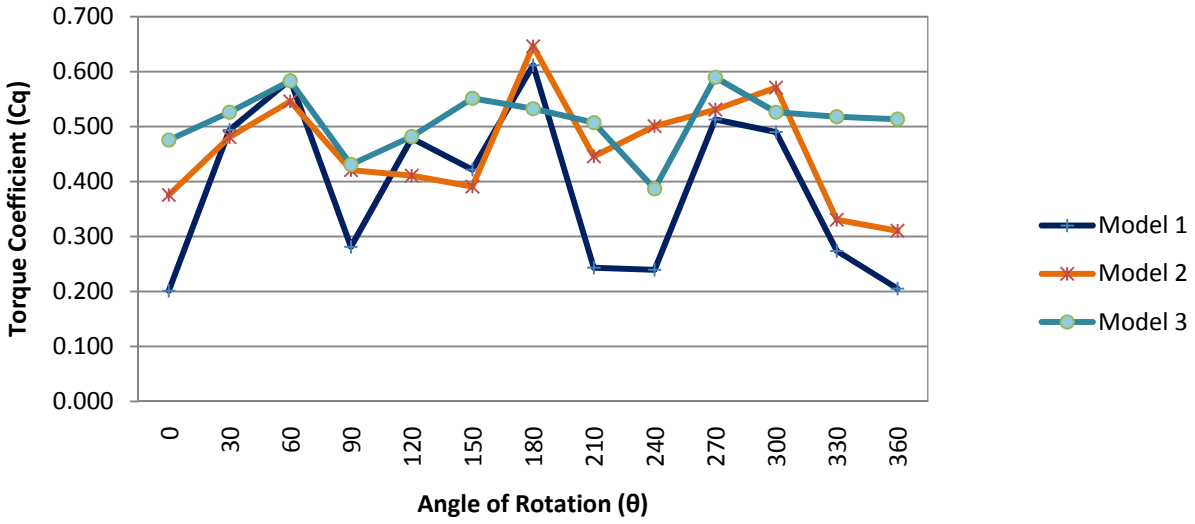

Figure 4.8: Torque Coefficient (C_q) versus Angle of Rotation (θ) at ***wind speed of 7.33 m/s.***

Comparisons of Experimental Torque Coefficient with Previous Research Results:

Figure 4.9 shows a comparison of experimental torque coefficient (C_q) variation of three models with the previous experimental results by Hayashi et al. [19]. They have used two bladed

Savonius wind turbine model with blade diameter, d =184 mm, overall rotor diameter, D = 330 mm, height, H = 230 mm and overlap ratio for the model was 0.2. They carried out the experiment at a wind speed of 9 m/s. Reynolds number used for their model was 2.10×10^5. For the current Model 1, Model 2 and Model 3 experiment was carried out at wind speed of 9.66 m/s and the corresponding Reynolds numbers were 1.61×10^5, 1.40×10^5, and 1.24×10^5 respectively. Currently the Reynolds number used in Model 1 is close to the Reynolds number of Hayashi et al. Model's and the two graphs show similar pattern for torque coefficient variation only difference is that for Hayashi Model torque coefficient variation graph shifted towards right than current Model 1. This difference is due to the fact that their model was two-bladed rotor whereas the current models all are three-bladed rotors. The maximum and minimum torque coefficient values are in very close match with the current study of Model 1.

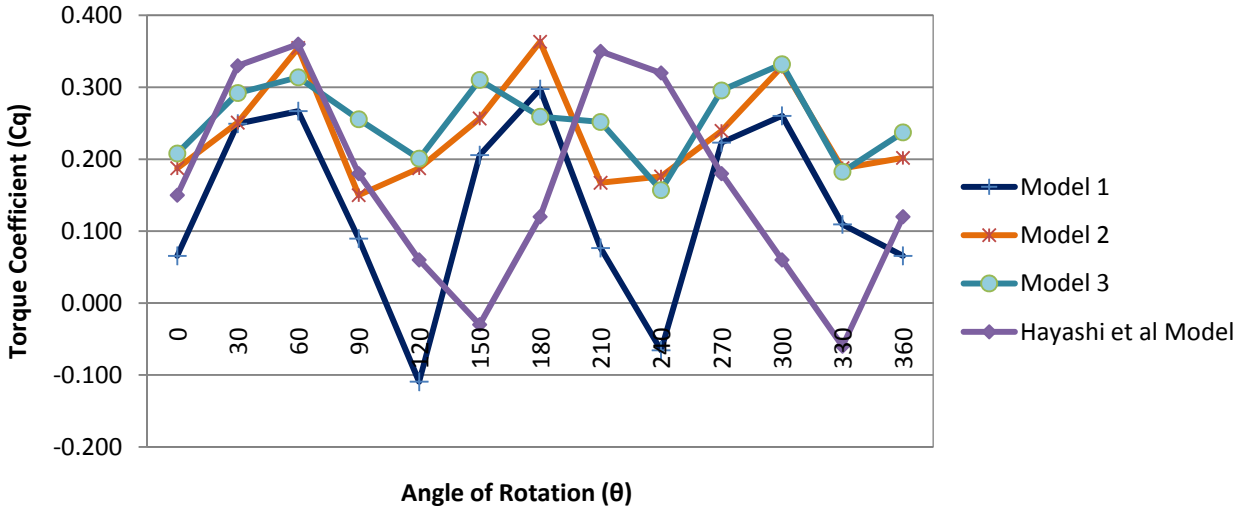

Figure 4.9: Comparison of Torque Coefficient (C_q) versus Angle of Rotation (θ).

Power Coefficient

Power Coefficient Variation for Three Individual Savonius VAWT Models:

Power coefficient (C_P) was calculated at three different Reynolds number (Re) for all three models. Figure 4.10 shows power coefficient (C_P) variation with angle of rotation (θ) from 0° to 360° for ***Model 1***. Trends of the plots are similar for Re = 1.61×10^5, 1.37×10^5 and 1.22×10^5. Power coefficient was negative at 120°, 210° and 240° for Re = 1.37×10^5 and at 120° and 240° for Re = 1.61×10^5. For this model, better power coefficient variation occurred at Re = 1.22×10^5. Figure 4.11 shows power coefficient (C_P) variation with angle of rotation (θ) at three different Reynolds number (Re) for ***Model 2***. There is no negative power coefficient for this model at any Reynolds number. Figure 4.12 shows power coefficient (C_P) variation with the change of angle of rotation (θ) from 0° to 360° for ***Model 3***. For this model, power coefficient variation follows the similar trend for all Reynolds number, increasing from 0° to 60° and then decreasing up to 120° then repeats from 120° to 230°and from 240° to 330°.

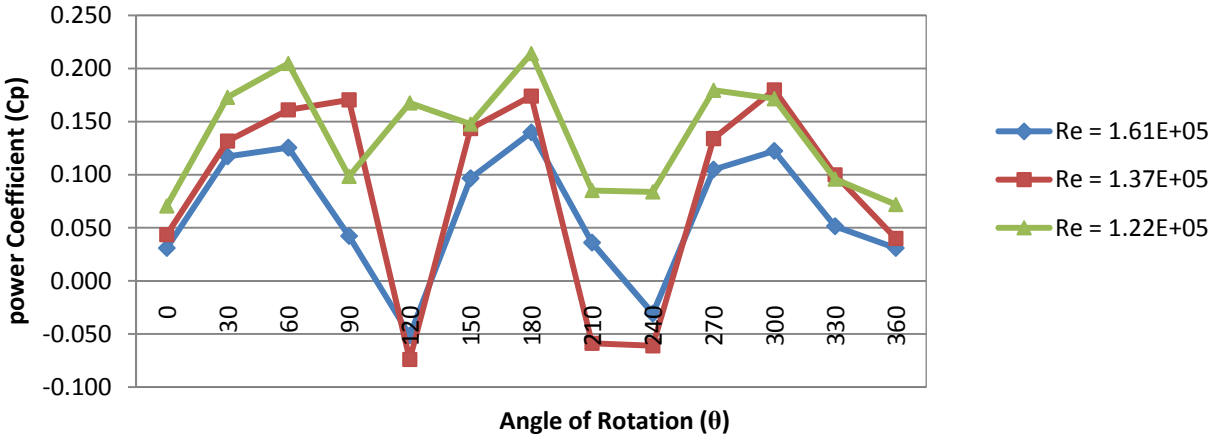

Figure 4.10: Power Coefficient (C_P) versus Angle of Rotation (θ) for ***Model 1***.

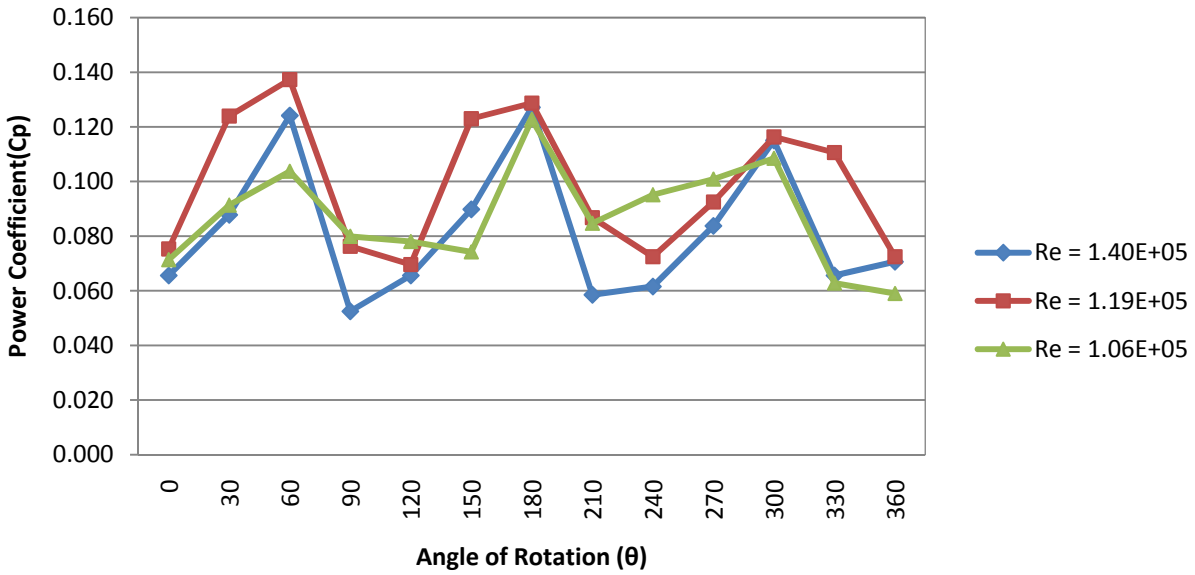

Figure 4.11: Power Coefficient (C_P) versus Angle of Rotation (θ) for ***Model 2***.

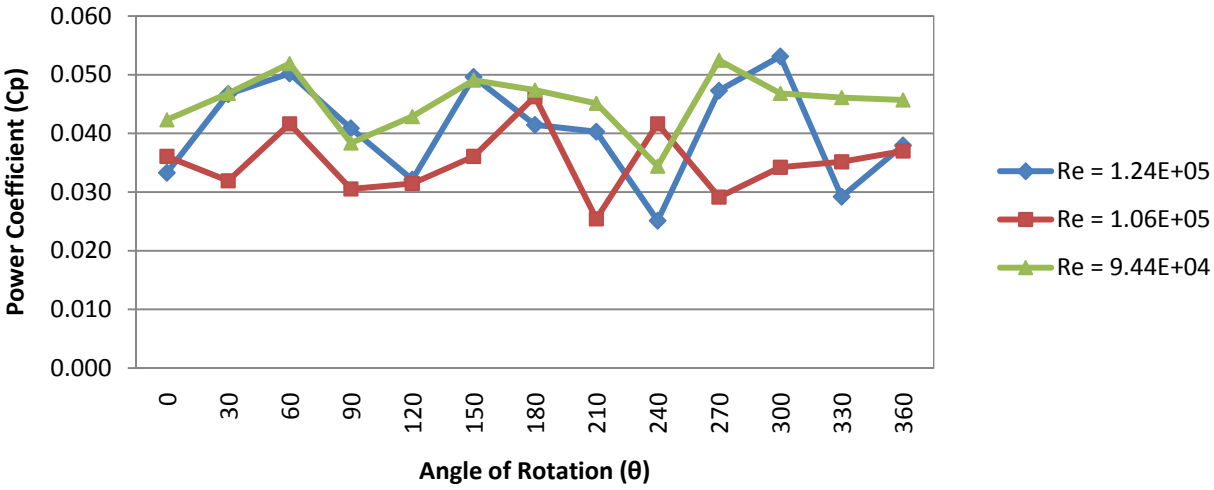

Figure 4.12: Power Coefficient (C_P) versus Angle of Rotation (θ) for ***Model 3***.

Power Coefficient Variation at Four Different Wind Speeds:

Figures 4.13 to 4.15 show power coefficient (C_P) variation with the increase of angle of rotation (θ) for three Savonius rotor models at three different wind speeds. Figure 4.13 shows C_P variation at wind speed of 9.66 m/s where improved power coefficient is observed for Model 2 and Model 3 than Model 1. Negative power coefficient values occur at rotor angle 120° and 240° for Model 1. Figure 4.14 shows that Model 2 and Model 3 demonstrate better power coefficients than Model 1 while wind speed is at 8.23 m/s and negative power coefficient occurs at rotor angle 120° and 240° for Model 1. Figure 4.15 shows that for all three rotor models power *coefficient remains positive with the increase of angle of rotation at wind speed of 7.33 m/s.*

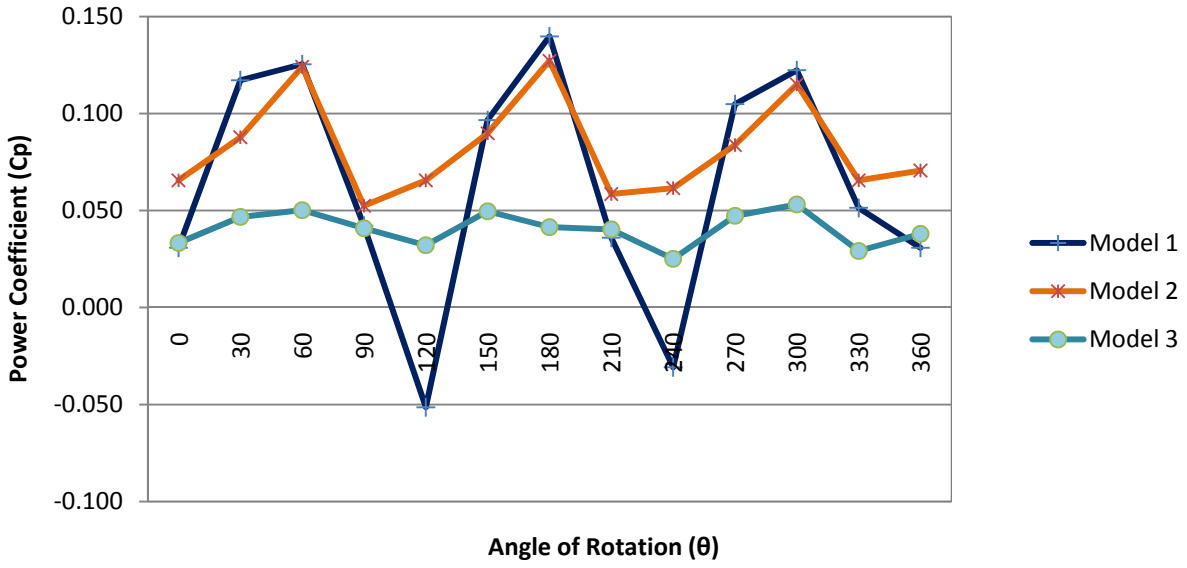

Figure 4.13: Power Coefficient (C_P) versus Angle of Rotation (θ) at ***wind speed 9.66 m/s***.

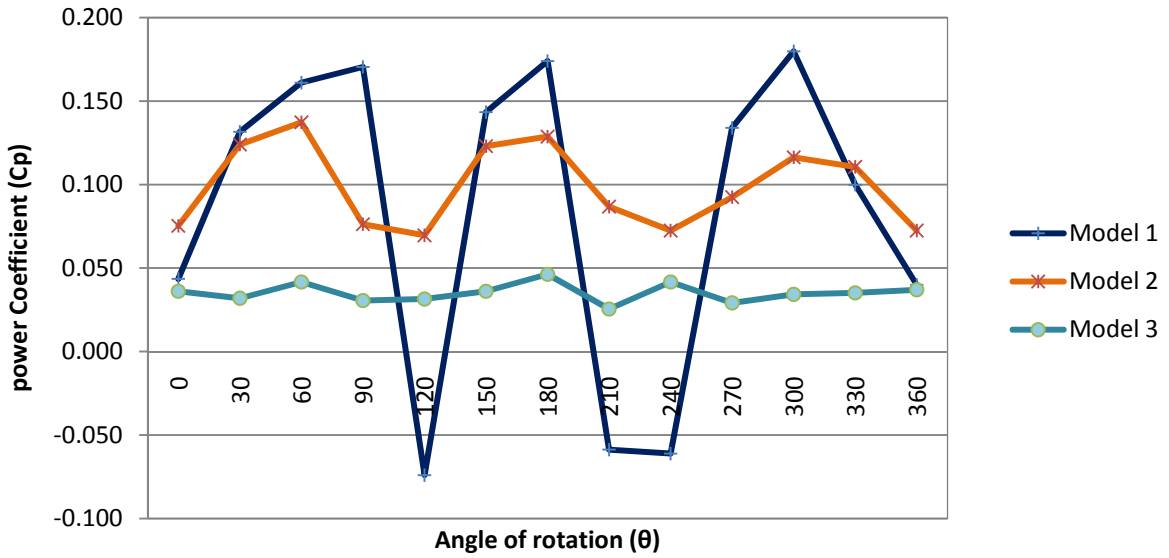

Figure 4.14: Power Coefficient (C_P) versus Angle of Rotation (θ) at ***wind speed 8.23 m/s***.

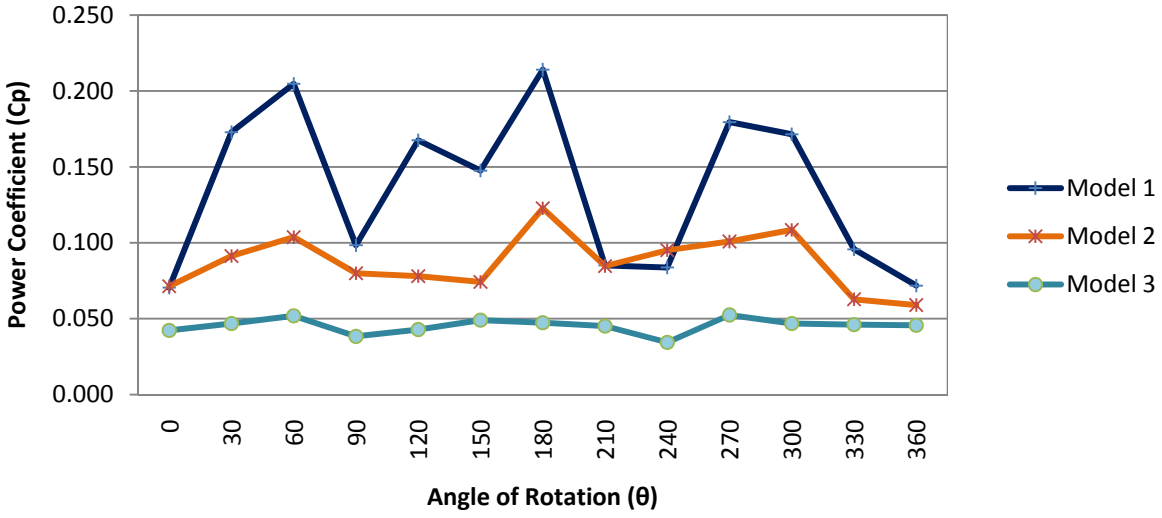

Figure 4.15: Power Coefficient (C_P) versus Angle of Rotation (θ) at ***wind speed 7.33 m/s***.

Numerical Results

Pressure Contours for Three Models at Three Different Reynolds Number

Pressure contours generated from numerical simulation of ***Model 1*** for three different Reynolds number are shown in Figures 4.16 to 4.18. For all these cases higher pressure values were found at the convex side of the first blade Savonius rotor model. Negative pressure region was developed from convex side of blade 2 to some portion of convex side of blade 3. This negative pressure is creating pressure difference between concave and convex surface that eventually rotates the turbine blades.

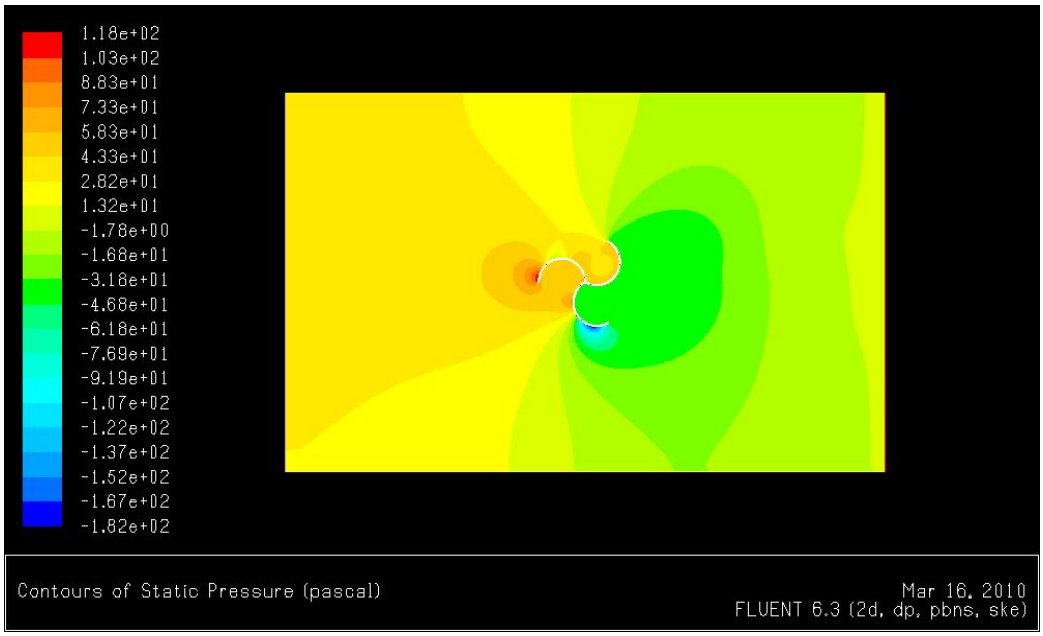

Figure 4.16: Pressure Contour around Savonius rotor Model 1 at Re = 1.61×10^5.

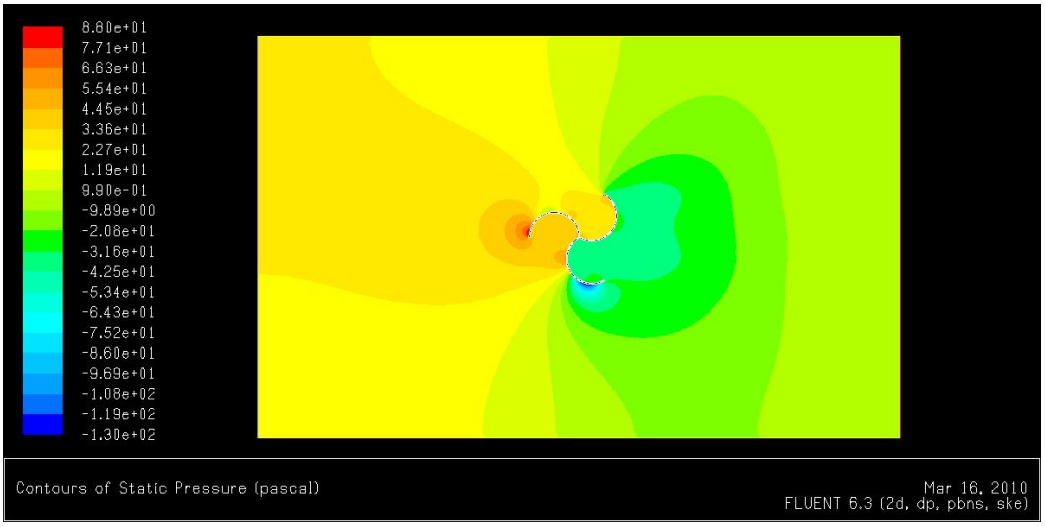

Figure 4.17: Pressure Contours around Savonius rotor Model 1 at Re = 1.37 $\times 10^5$.

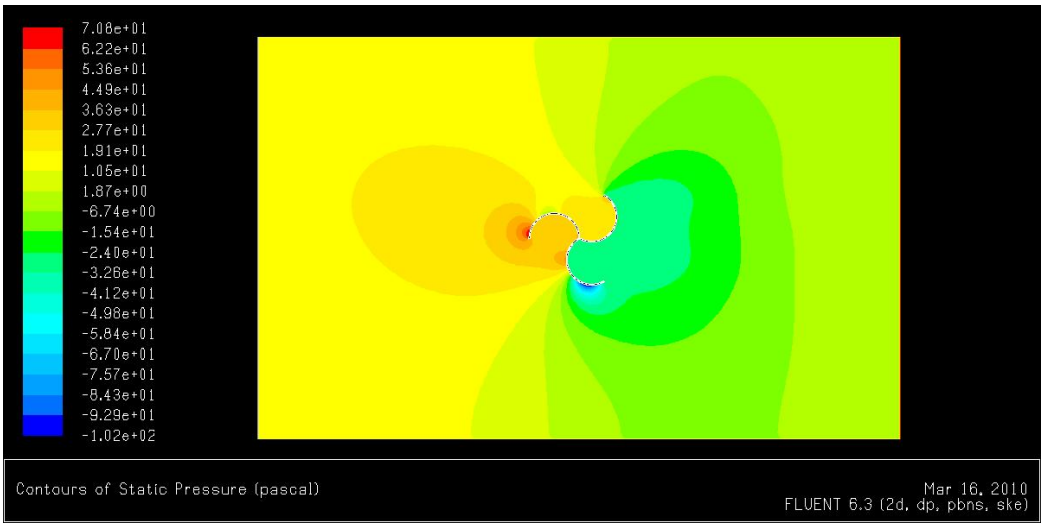

Figure 4.18: Pressure Contour around Savonius rotor Model 1 at Re = 1.22 $\times 10^5$.

Pressure contours around the Savonius rotor ***Model 2*** at three different Reynolds number are shown in Figures 4.19 to 4.21. Likewise Model 1 pressure contours the higher pressure region was developed at convex side of blade 1 and most negative pressure region was

developed at outside of convex side of blade 3. Pressure contours around the Savonius rotor ***Model 3*** are shown in Figures 4.22 to 4.24.

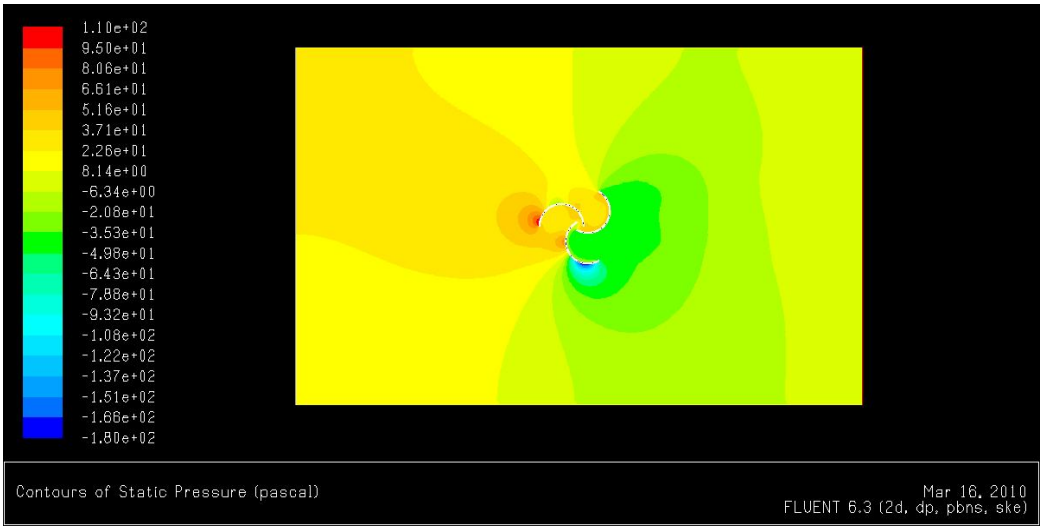

Figure 4.19: Pressure Contour around Savonius rotor Model 2 at Re = 1.40 $\times 10^5$.

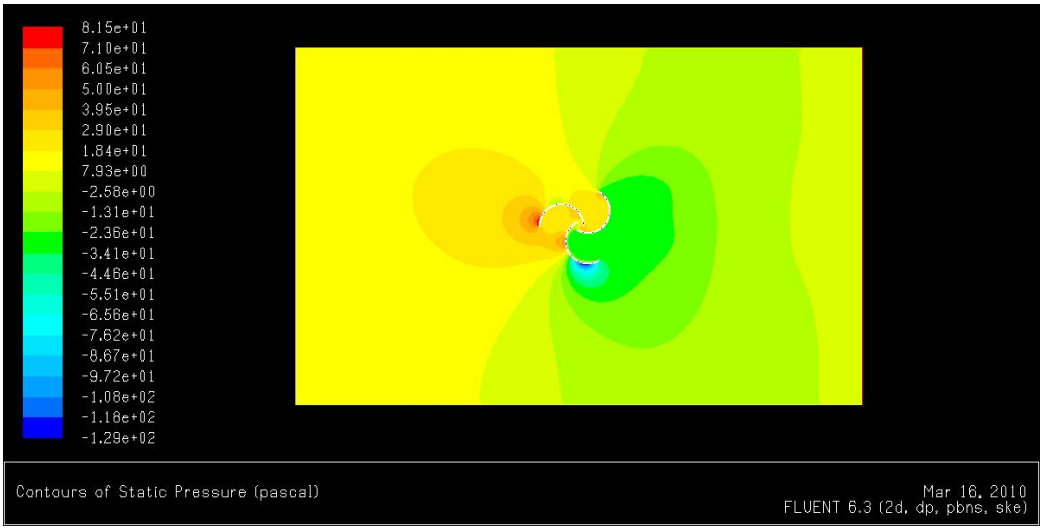

Figure 4.20: Pressure Contour around Savonius rotor Model 2 at Re = 1.19 $\times 10^5$.

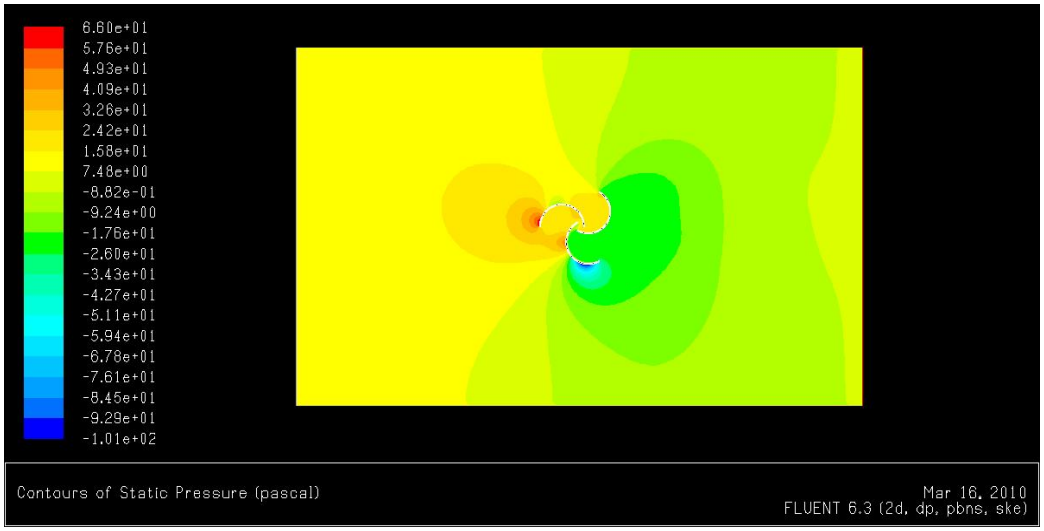

Figure 4.21: Pressure Contour around Savonius rotor Model 2 at Re = 1.06 $\times 10^5$.

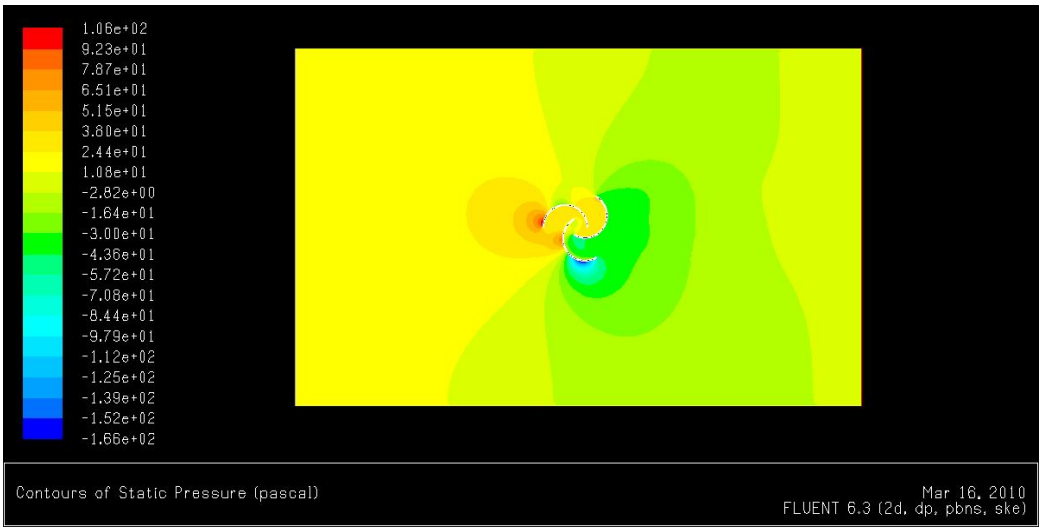

Figure 4.22: Pressure Contour around Savonius rotor Model 3 at Re = 1.24 $\times 10^5$.

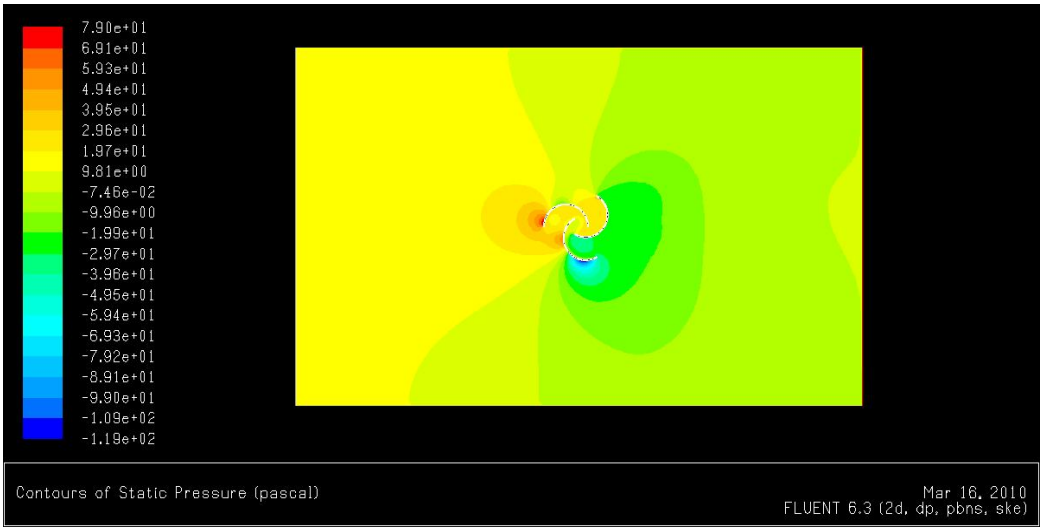

Figure 4.23: Pressure Contour around Savonius rotor Model 3 at Re = 1.06 $\times 10^5$.

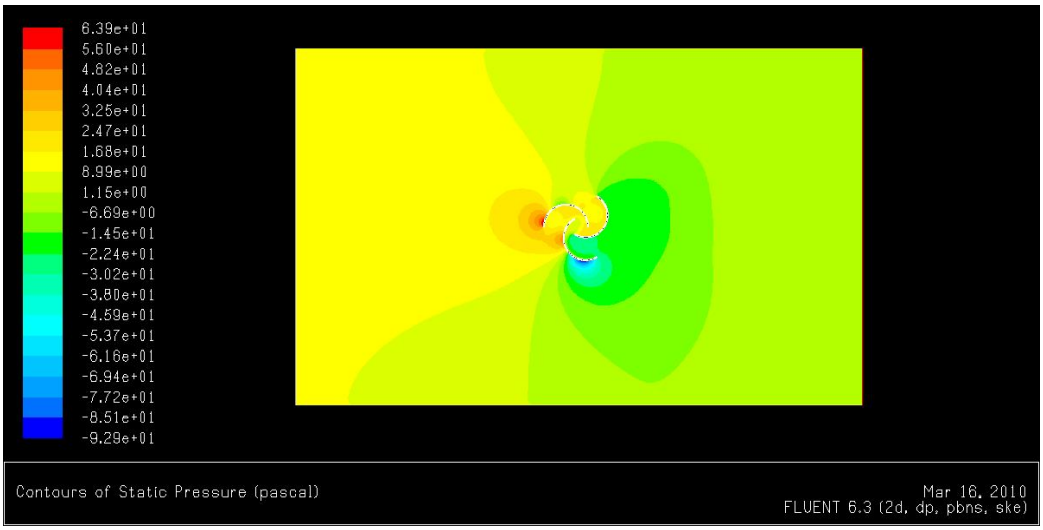

Figure 4.24: Pressure Contour around Savonius rotor Model 3 at Re = 9.44 $\times 10^4$.

Velocity Contours for Three Models at Three Different Reynolds Number

Contours of Velocity magnitude for Savonius rotor ***Model 1*** at three different Reynolds number are shown in Figures 4.25 to 4.27. Patterns of the contours are almost same for different Reynolds number only exception is a slight variation in velocity magnitude. Once the wind strikes the turbine blades the velocity starts to decrease at the trailing edge of the Savonius wind turbine model but after some distance travel stars to regain the velocity. Higher velocity region was created at the top and bottom side of the wind turbine model. Figures 4.28 to 4.30 show velocity contours for ***Model 2*** and Figures 4.31 to 4.33 show velocity contours for ***Model 3*** at different Reynolds number. Similar patterns of velocity contours are observed for Model 2 and Model 3 but only the velocity magnitudes are different for different model cases. From these figures it can be seen that with the increase of overlap ratio the lower velocity region shorten after the trailing edge and come closer to the turbine blades.

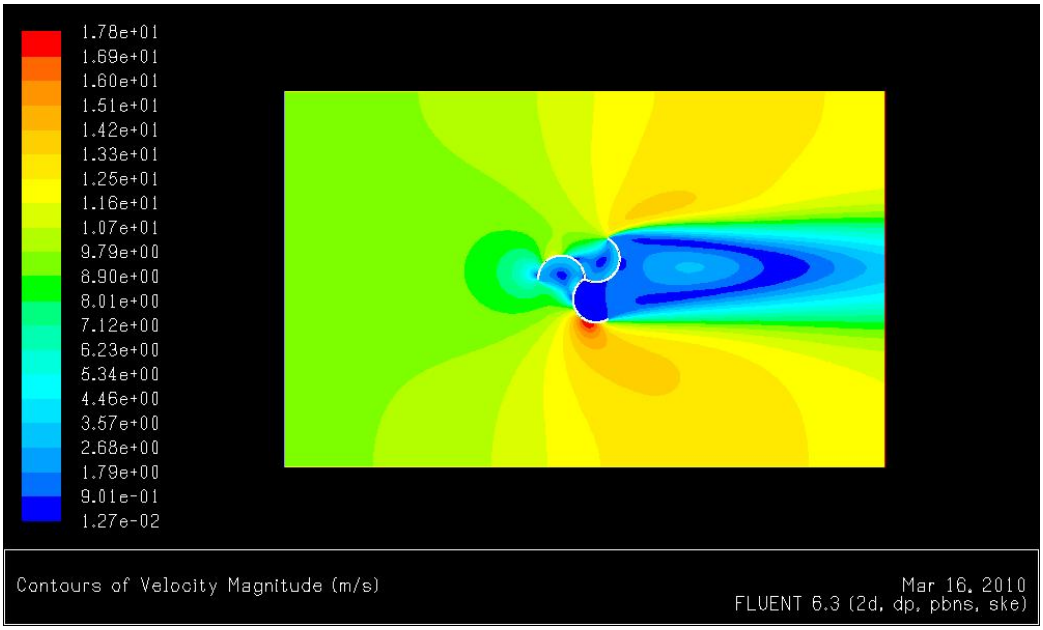

Figure 4.25: Velocity Contour around Savonius rotor Model 1 at Re = 1.61×10^5.

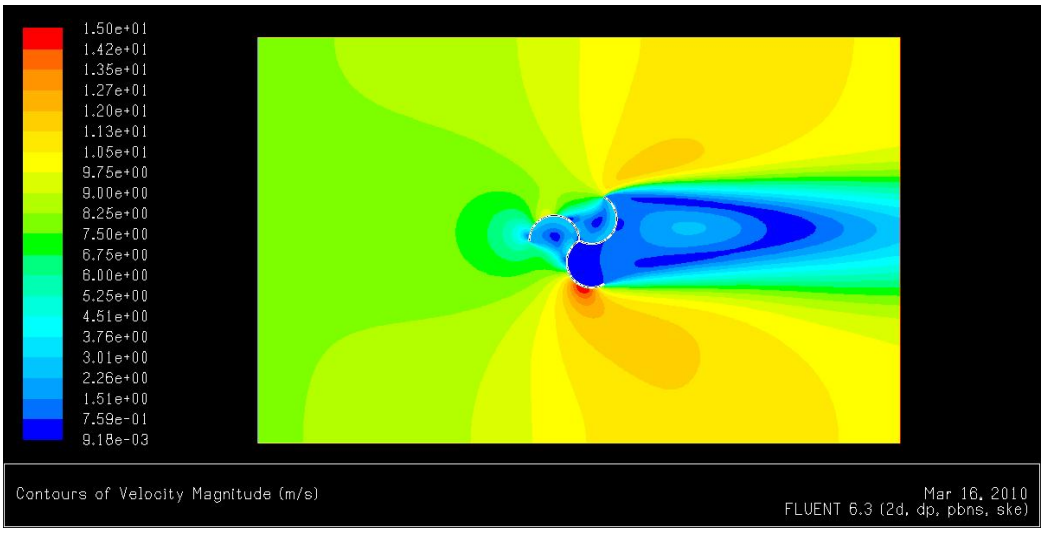

Figure 4.26: Velocity Contour around Savonius rotor Model 1 at Re = 1.37×10^5.

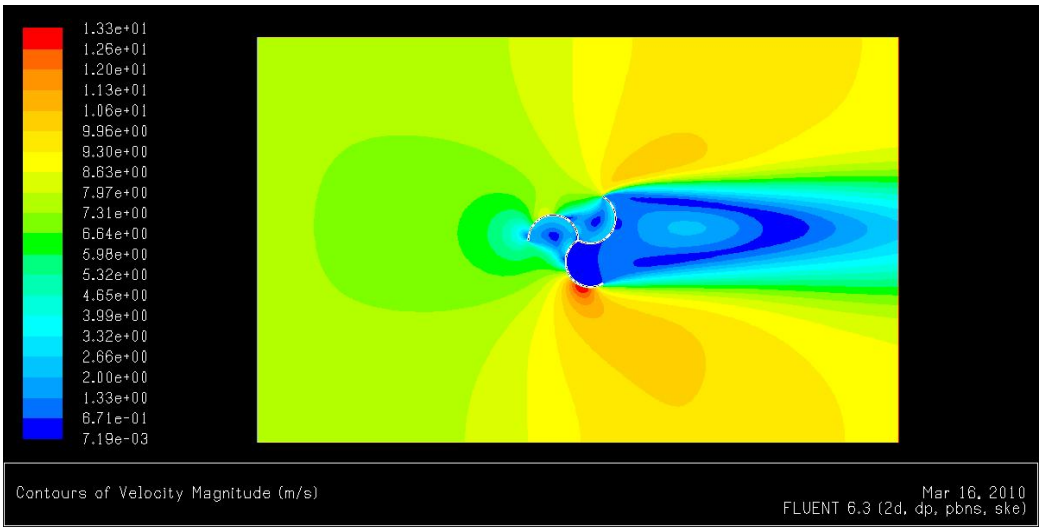

Figure 4.27: Velocity Contour around Savonius rotor Model 1 at Re = 1.22×10^5.

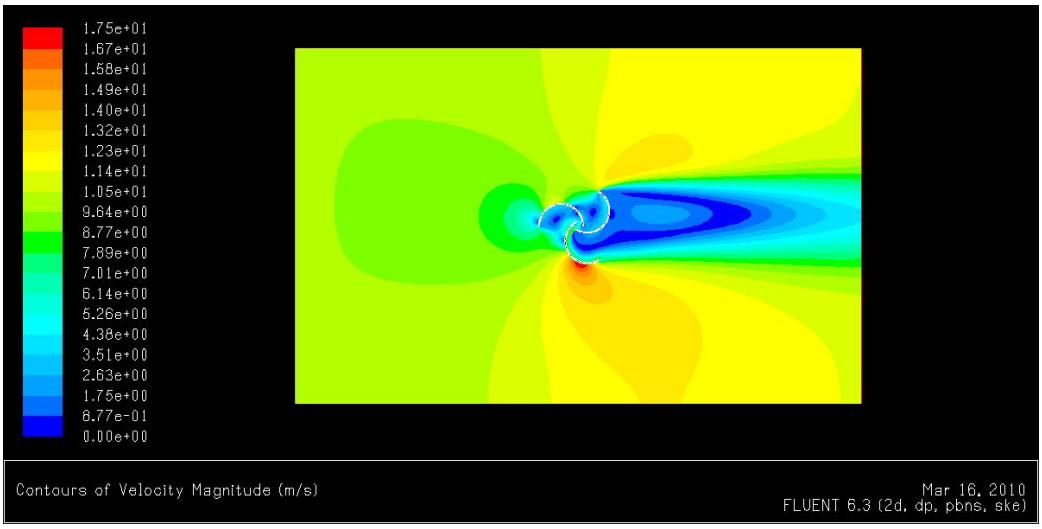

Figure 4.28: Velocity Contour around Savonius rotor Model 2 at Re = 1.40 $\times 10^5$.

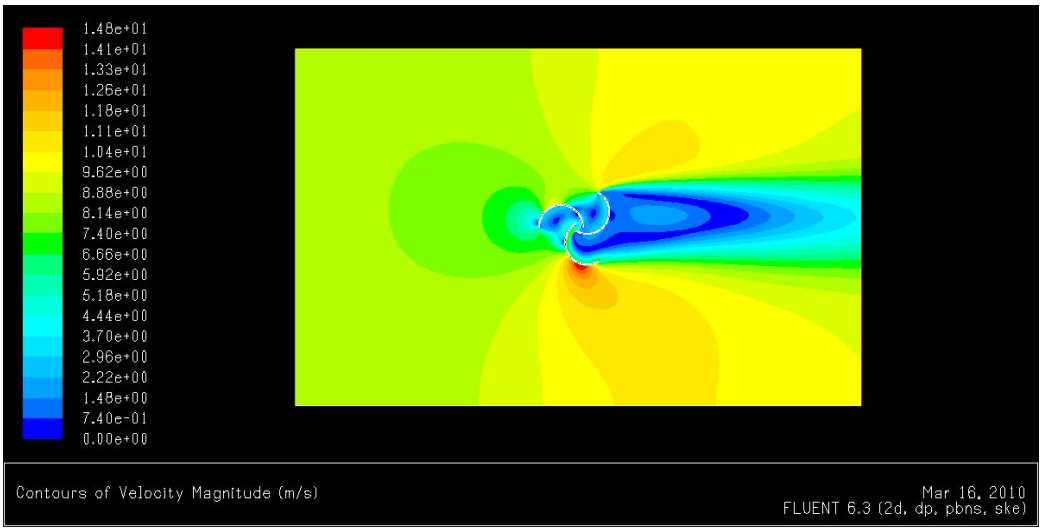

Figure 4.29: Velocity Contour around Savonius rotor Model 2 at Re = 1.19 $\times 10^5$.

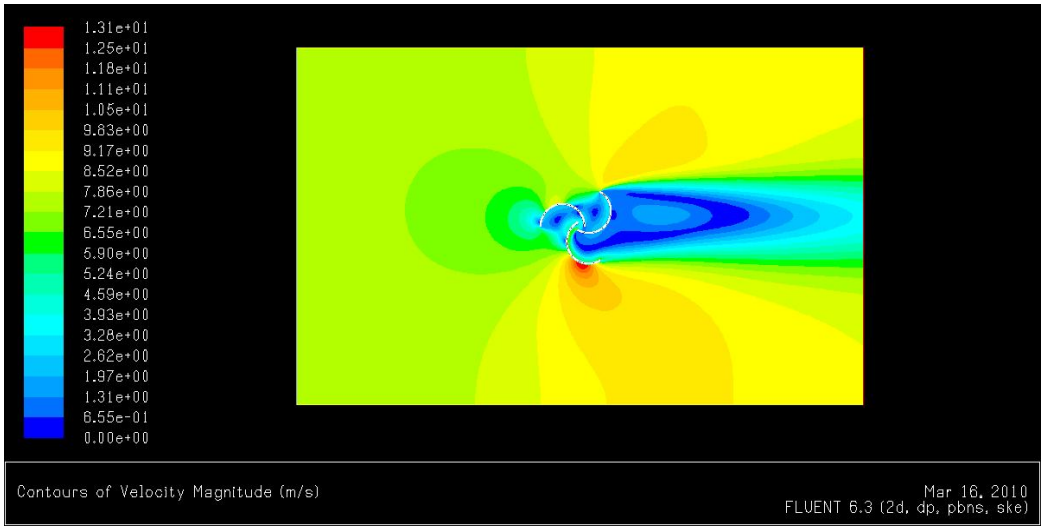

Figure 4.30: Velocity Contour around Savonius rotor Model 2 at Re = 1.06 $\times 10^5$.

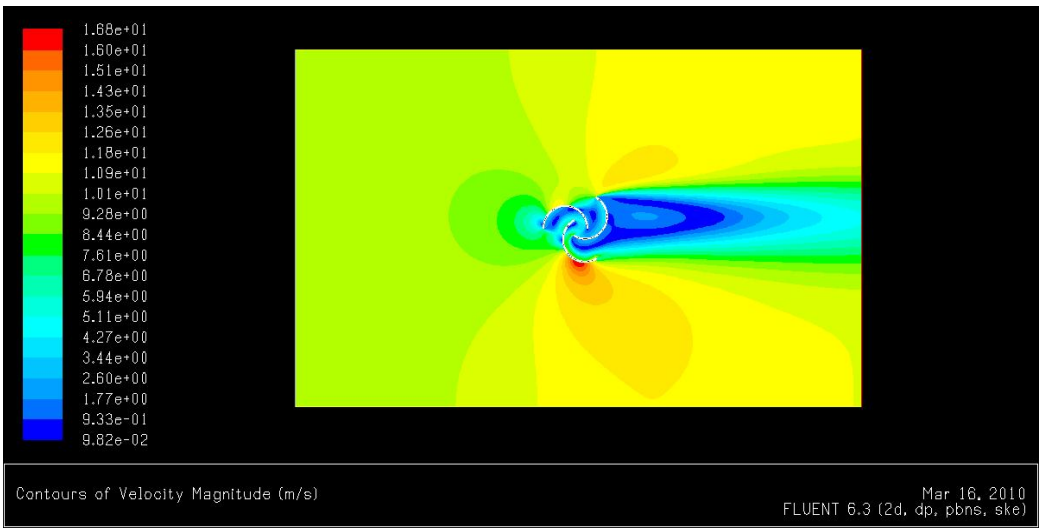

Figure 4.31: Velocity Contour around Savonius rotor Model 3 at Re = 1.24 $\times 10^5$.

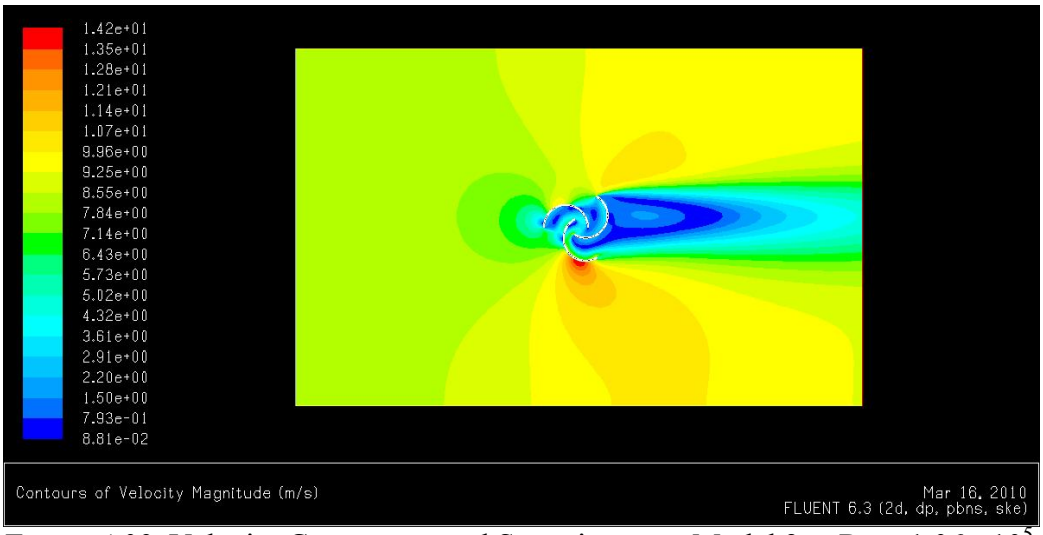

Figure 4.32: Velocity Contour around Savonius rotor Model 3 at Re = 1.06 $\times 10^5$.

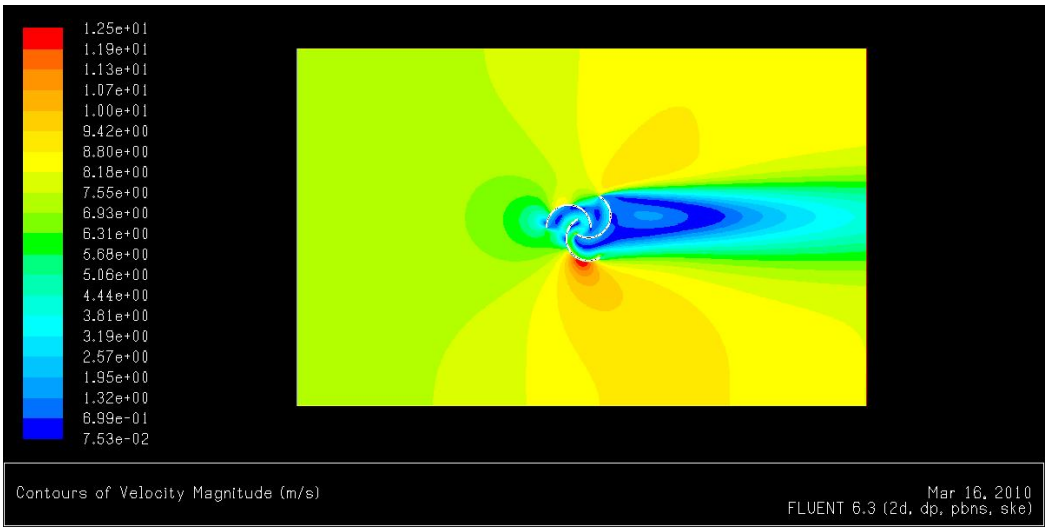

Figure 4.33: Velocity Contour around Savonius rotor Model 3 at Re = 9.44 $\times 10^4$.

Torque Coefficient (C_q)

Figure 4.34 shows the numerically calculated torque coefficient (C_q) variation with different Reynolds number (Re) for three different models. With the increase of Reynolds number torque coefficient slightly increases for all three models. Model 1 gives better torque coefficient compared to other two models.

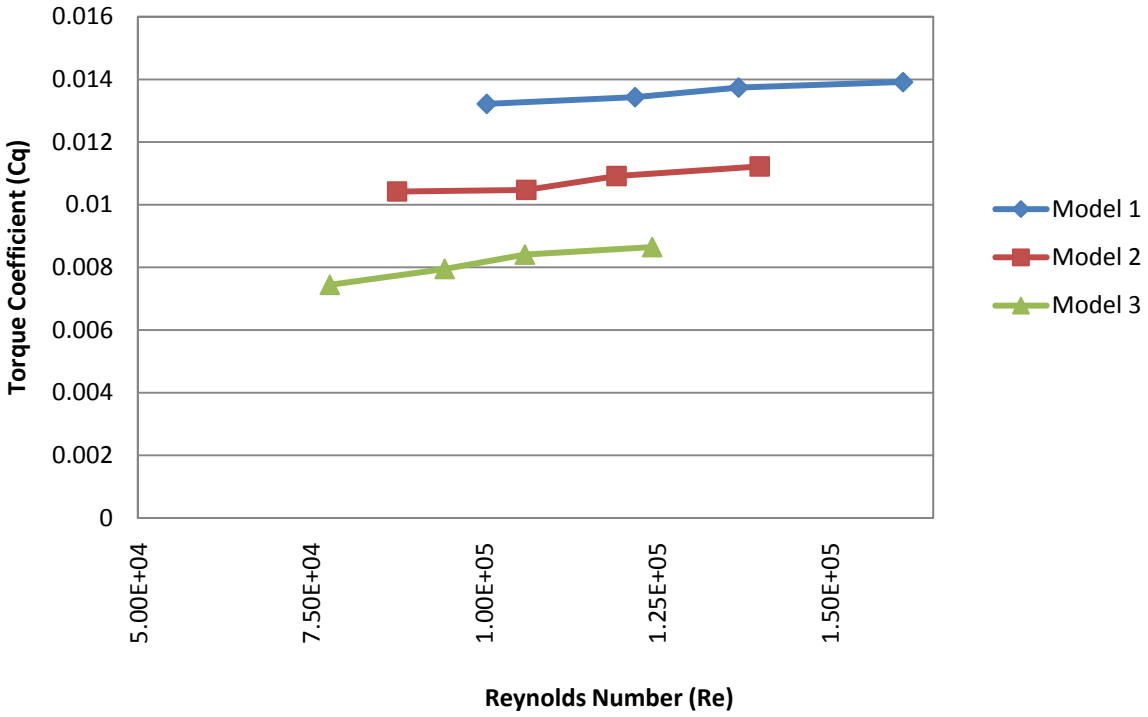

Figure 4.34: Torque Coefficient (C_q) versus Reynolds number (Re) for three Models.

Comparison of Numerical and Experimental Power Coefficient

Figure 4.35 shows the comparison of numerically and experimentally calculated power coefficient (C_P) of the three Savonius rotor Models with the increase of tip speed ratio (λ). Converged solutions of the power coefficient values were considered at all tip speed ratios for

numerical results whereas power coefficient at four rotor positions 0°, 30°, 60° and 90° were considered for experimental values. Combined blade effect was considered for both experimental and numerical calculation. Figure 4.35 shows that for Model 1 experimental power coefficient at rotor position 0° is very close to the numerical results. But the deviation is huge for rotor position 60°. This may be during experiment there was disturbance from environment which causes sudden power increase and also in numerical simulation the boundary effect causes lower numerical value. Similar pattern of power coefficient variation is observed for Model 2 and Model 3 as shown in Figures 4.36 and 4.37. But the magnitude of the C_P decreases for Model 2 and Model 3 for both numerical and experimental cases.

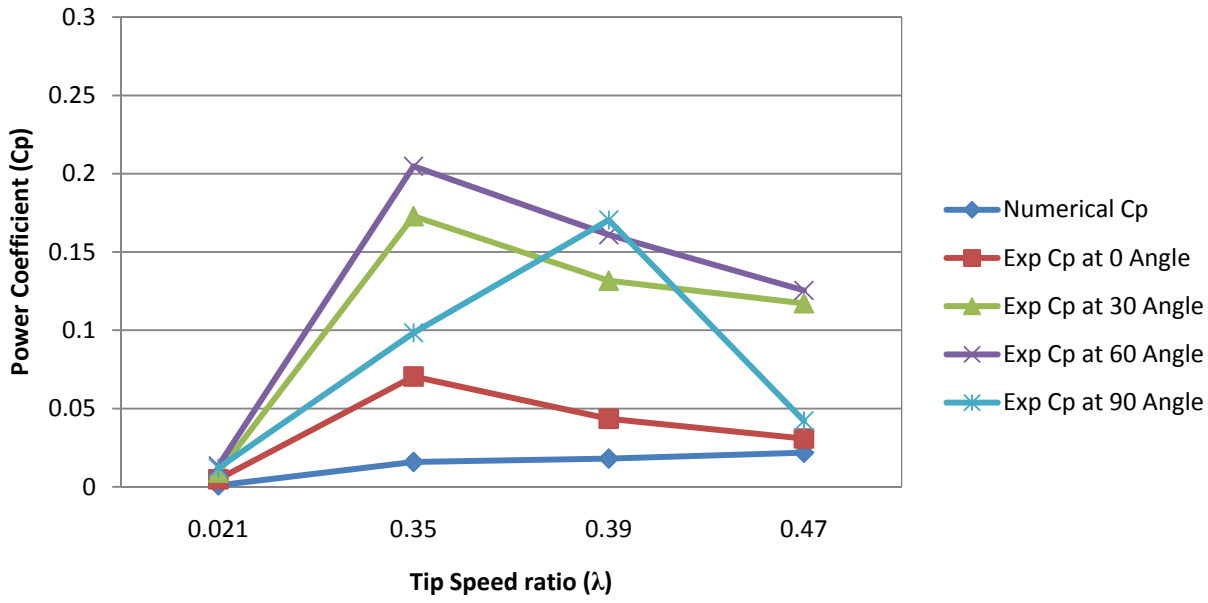

Figure 4.35: Power Coefficient (CP) versus Tip speed ratio (λ) for Model 1.

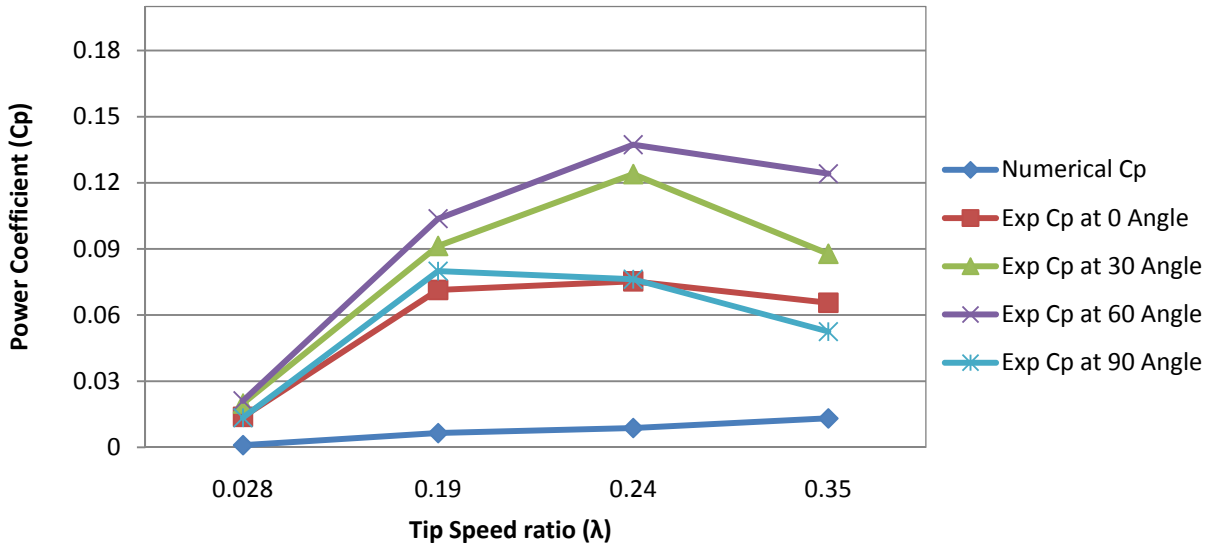

Figure 4.36: Power Coefficient (C_P) versus Tip speed ratio (λ) for Model 2.

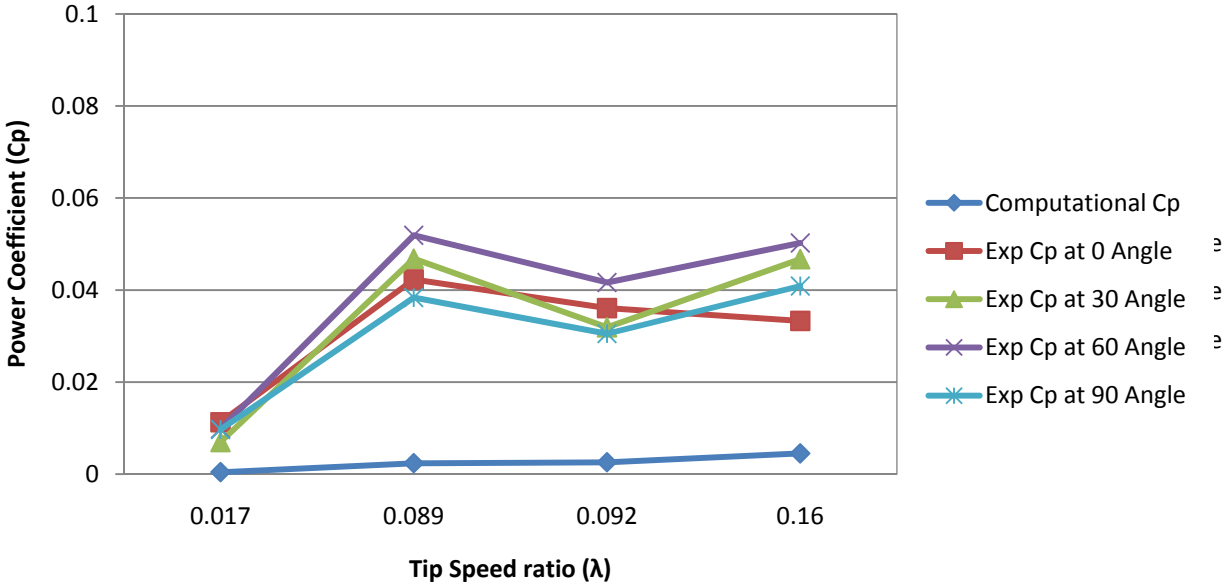

Figure 4.37: Power Coefficient (C_P) versus Tip speed ratio (λ) for Model 3.

CHAPTER 5

CONCLUSION AND RECOMMENDATION

Introduction

Three different three bladed Savonius wind turbine scale models with different overlap ratios (Model 1: no overlap, Model 2: overlap ratio 0.12 and Model 3: overlap ratio 0.26) were designed and fabricated for the current study. Aerodynamic characteristics of these models were experimentally investigated using the subsonic wind tunnel. Experimental investigation was performed at different Reynolds numbers. Numerical investigation was also performed to determine torque and power coefficients using GAMBIT and FLUENT.

Conclusion

From this current study, analysis and results of this research work, the following conclusions can be made:

i. For Model 1 with Re = 1.22×10^5, Model 2 with Re = 1.06×10^5, and Model 3 with Re = 9.94×10^4 experimental torque coefficient (C_t) shows higher and positive values compared to other Reynolds numbers. It also shows that lower Reynolds number gave better torque coefficient (C_t) variation with the increase of the angle of rotation for each Model. Model 2 demonstrate better experimental torque coefficient (C_t) for all three different wind speeds (9.66 m/s, 8.23 m/s, and 7.33 m/s).

ii. For Model 1 with Re = 1.22×10^5, Model 2 with Re = 1.19×10^5, and Model 3 with Re = 9.94×10^4 experimental power coefficient (C_P) shows higher and positive values compared to other Reynolds numbers. Model 2 shows the better experimental power

coefficient (C_P) at wind speed 9.66 m/s and wind speed 8.23 m/s. But for wind speed 7.33 m/s Model 1 shows the better power coefficient (C_P).

iii. With the increase of Reynolds number numerical torque coefficient increases for all three Models.

iv. Power coefficient calculated from numerical method shows that it is always increasing with the increase of tip speed ratio. For Model 1 numerical power coefficient matches well with the corresponding experimental values at 0° rotor position.

Suggestion of future work

Following suggestions can be made for further improvement of the current research:

- Present study was conducted for tip speed ratios from 0.017 to 0.47 and for Reynolds numbers from 7.78×10^4 to 1.61×10^5. For future study it is recommended that investigation can be perform for higher tip speed ratios for better understanding of the change of power and torque characteristics variation with higher tip speed ratios.
- Also the effect of aerodynamic characteristic can be observed at higher Reynolds numbers. For this, a modified subsonic wind tunnel which will have the option of variable wind speed as well as higher velocity limit is strongly recommended for better experimental investigation.
- Dynamic torque can be measured using the dynamic torque tester for better results and thus an efficient model can be designed and improved results can be obtained.
- Better aerodynamic performance can be achieved by improving the VAWT design by optimizing the blade shape and blade numbers.

- Investigation can be made by combining the two types of vertical axis wind turbine (VAWT) like Darrious and Savonius wind turbine to overcome the negative torque generated during the rotation.

BIBILOGRAPHY

[1] Aldoss, T. K., Obeidat, K. M. (1987) Performance analysis of two Savonius rotors running side by side using the discrete vortex method, Wind Engineering, 11, 79-88.

[2] Altan, B. D., Atilgan, M. (2008). An experimental and numerical study on the improvement of the performance of savonius wind rotor. *Energy conversion and management,* 3425-3432.

[3] Altan, B. D., Atilgan, M, Ozdamar, A. (2008). An Experimental study on improvement of a savonius rotor performance with curtaining. *Experimental thermal and fluid science,* 32, 1673-1678

[4] Benjanirat, S., Sankar, L., & Xu, G. (2003). Proceedings of 41st aerospace sciences meeting and exhibit *Evaluation of turbulence models for the prediction of wind turbine aerodynamics*. Reno, Nevada.

[5] Diaz, F., Gavalda, J., Massons, J. (1991) Drag and lift coefficients of the Savonius wind machine, *Journal of Wind Engineering.* 15, 240-246.

[6] Fluent 6.3 user guide

[7] Fujisawa , N. (1992). On torque mechanism of savonius rotors. *Journal of Wind Engineering and Industrial Aerodynamics,* 40, 227-292

[8] Fujisawa, N., Gotoh, F. (1994) Experimental study on the aerodynamic performance of a Savonius rotor, *ASME Journal of solar energy engineering*, 116, 148 – 152.

[9] Gupta, R., Biswas, A., Sharma, K. K. (2008). Comparative study of a three bucket savonius rotor with a combined three bucket savonius –three bladed darrieus rotor. *Rnewable Energy,* 33, 1974-1981

[10] Hau, E. (2006) *Wind turbines: Fundamentals, technologies, applications, economics*. Germany. Springer- verlag berlin Heidelberg.

[11] Hayashi, T., Li, Y., Hara, Y., Suzuki (2004) Proceedings of European Wind Energy Conference and Exhibition, *Wind tunnel test on a three stage out phase Savonius rotor,* London, England.

[12] Hayashi, T. , Li, Y., Hara, Y. (2005). Wind tunnel tests on a different phase three stage savonius rotor. *JSME international journal,* 48, 9-16.

[13] Islam, A. K. M. S., Islam, M. Q., Razzaque, M. M.,& Ashraf, R., (1995), Static Torque and Drag Characteristics of an S-shaped Savonius Rotor and Prediction of Dynamic Characteristics, *Wind Engineering*, 19.

[14] Kamoji, M.A. , Kedare, S.B. , Prabhu, S.V. (2009). Performance test of helical savonius rotors. *Renewable Energy,* 34, 521-529

[15] Kamoji, M. A., Kedare, S. B. (2007) Proceedings of 5th AIAA International Energy Conversion Engineering Conference. *Wind tunnel tests on a single stage helical Savonius rotor*.

[16] Launder, B. E. and Spalding, D. B.(1972) Lectures in Mathematical Models of Turbulence. Academic Press.

[17] Lida, A., Kato, K. & Mizuno, A.(2007). Proceedings of 16th Australasian fluid mechanics conferences. *Numerical simulation of unsteady flow and aerodynamic performance of vertical axis wind turbine with LES.* Gold Coast, Australia.

[18] McWilliam, M., Johnson, D.A. (2008). Velocity measurement of flow around model vertical axis wind turbines. *International Journal of Green Energy,*5, 55-68.

[19] Menet, J.L., Bourabaa, N. (2004). Proceedings of European Wind Energy Conference. *Increase in the Savonius Rotor Efficiency via a Parametric Investigation.* London, UK

[20] Menet, J.L., Valdes, L.C., Menart, B. (2001). A comparative calculation of the wind turbines capacities on a basis of the L-σ criterion, *Renewable Energy,* 22, 491-506.

[21] Newman, B. G. (1974). Proceedings of symposium on wind energy: achievements and potential. *Measurements on a savonius rotor with a variable gap.* Sherbrooke, Canada.

[22] Patankar, S. V., (1980) Numerical Heat Transfer and Fluid Flow, Hemisphere Publishing Corporation.

[23] Paraschivoiu, I. (2002). *Wind turbine design: with emphasis on Darrieus concept*. Montreal, Canada: Polytechnic International Press.

[24] Pike Research LLC (2009). *Wind Energy Outlook for North America Wind Power Generation Capacity and Turbine Deployments: Market Analysis and Forecasts.* Boulder, CO. : Beh, G. , Wheelock, C.

[25] Pinkerton, R. B. (1936). Calculated and measured Pressure distribution over the midspan section of the NACA 4412 airfoil. NACA report no 563. 365-380

[26] Rahman, M., Islam, M. Q., Islam, A.K.M.S. (1999) Proceeding of the third international conference on fluid mechanics and heat transfer. *Prediction of dynamic characteristics of a three bladed Savonius rotor.*

[27] Rahman, M. (1999) Torque and drag characteristics of a three bladed Savonius rotor, M. Sc. Thesis, Mech. Eng. Dept., Bangladesh University of Eng. and Tech., Bangladesh.

[28] Rahman, M., Islam, M. Q., Islam, A.K.M.S. (1999) Proceeding of the 2nd int. seminar on renewable energy for poverty alleviation, IEB, Bangladesh, *Aerodynamic characteristics of a three bladed Savonius rotor*.

[29] Riegler, H. (2003). HAWT versus VAWT, Retrieved from http://www.victordanilochkin.org/research/turbine/papers/HAWT%20versus.pdf

[30] Saha, U. K., Thotla, S., Maity, D. (2008). Optimum design configuration of Savonius rotor through wind tunnel experiment. *Journal of wind engineering and industrial aerodynamics.* 96, 1359-1375.

[31] Sargolzaei, J., Kianifar, A. (2009). Modeling and simulation of wind turbine savonius rotor using artificial neural networks for estimation of the power ratio and torque. *Simulation modeling practice and theory.* 17, 1290-1298

[32] Savonius, S. J. (1931). The S rotor and its application. *Mechanical Engineering,* 53, 333-338.

[33] Sawada, T., Nahamura, M., Kamada, S. (1986) Blade force measurement and flow visualization of Savonius rotors, *Bulletin of JSME*, 29, 2095-2100.

[34] Shepherd, D. G. (1990). Historical Development of the windmill. National Aeronautics and Space Administration office of management.

[35] U. S. Department of Energy (2008). 20% wind energy by 2030: Increasing wind energy's contribution to U.S. electricity supply. (DOE/GO-102008-2567)

[36] Worldwatch Institute (2008). *Renewables 2007: Global Status Report*. Washington, DC. : Martinot , E.

[37] Wulff, H. E., (1966). The traditional crafts of Persia, their development, technology and influence on eastern and western civilization.MIT press. 284-289